

1997

An investigation of the flow over a flat plate at incidence with a vortex/sink combination

Marcus Brooks
San Jose State University

Follow this and additional works at: https://scholarworks.sjsu.edu/etd_theses

Recommended Citation

Brooks, Marcus, "An investigation of the flow over a flat plate at incidence with a vortex/sink combination" (1997). *Master's Theses*. 1424.

DOI: <https://doi.org/10.31979/etd.w4tc-cva8>

https://scholarworks.sjsu.edu/etd_theses/1424

This Thesis is brought to you for free and open access by the Master's Theses and Graduate Research at SJSU ScholarWorks. It has been accepted for inclusion in Master's Theses by an authorized administrator of SJSU ScholarWorks. For more information, please contact scholarworks@sjsu.edu.

INFORMATION TO USERS

This manuscript has been reproduced from the microfilm master. UMI films the text directly from the original or copy submitted. Thus, some thesis and dissertation copies are in typewriter face, while others may be from any type of computer printer.

The quality of this reproduction is dependent upon the quality of the copy submitted. Broken or indistinct print, colored or poor quality illustrations and photographs, print bleedthrough, substandard margins, and improper alignment can adversely affect reproduction.

In the unlikely event that the author did not send UMI a complete manuscript and there are missing pages, these will be noted. Also, if unauthorized copyright material had to be removed, a note will indicate the deletion.

Oversize materials (e.g., maps, drawings, charts) are reproduced by sectioning the original, beginning at the upper left-hand corner and continuing from left to right in equal sections with small overlaps. Each original is also photographed in one exposure and is included in reduced form at the back of the book.

Photographs included in the original manuscript have been reproduced xerographically in this copy. Higher quality 6" x 9" black and white photographic prints are available for any photographs or illustrations appearing in this copy for an additional charge. Contact UMI directly to order.

UMI

A Bell & Howell Information Company
300 North Zeeb Road, Ann Arbor MI 48106-1346 USA
313/761-4700 800/521-0600

**An Investigation of the Flow over a Flat Plate at
Incidence with a Vortex/Sink Combination**

A Thesis

Presented to

The Faculty of the Department of Mechanical and Aerospace Engineering

San Jose State University

In Partial Fulfillment

of the Requirements for the Degree

Master of Science

by

Marcus Brooks

May 1997

UMI Number: 1384673

**Copyright 1997 by
Brooks, Marcus**

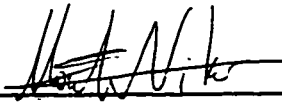
All rights reserved.

**UMI Microform 1384673
Copyright 1997, by UMI Company. All rights reserved.**

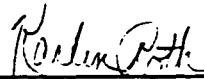
**This microform edition is protected against unauthorized
copying under Title 17, United States Code.**

UMI
300 North Zeeb Road
Ann Arbor, MI 48103

APPROVED FOR THE DEPARTMENT OF
MECHANICAL AND AEROSPACE ENGINEERING



Dr. Nikos Mourtos

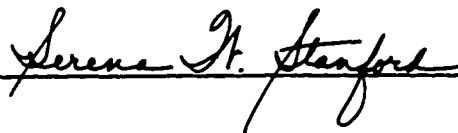


Dr. Karlin Roth



Dr. Dick Desautel

APPROVED FOR THE UNIVERSITY



© 1997

Marcus Brooks

ALL RIGHTS RESERVED

ABSTRACT

An Investigation of the Flow over a Flat Plate at Incidence with a Vortex/Sink Combination

By Marcus Brooks

A smoke visualization experiment was performed in the smoke tunnel of the aerodynamics laboratory at San Jose State University to study the vortex formation over a flat plate at an angle of attack. Suction was applied in the spanwise direction over the flat plate in an effort to create a stable vortex at locations and strengths predicted analytically from a two-dimensional, steady, incompressible, and inviscid model. Other promising locations were also tried and a trial-and-error approach was used to find the strongest and most stable vortices. Although the agreement between theory and experiment was limited, a variety of stable vortex locations were discovered experimentally behind the leading edge of the plate for relatively low suction rates. A computational analysis was also performed using an incompressible Navier-Stokes code, INS2D. The solutions generated by INS2D were in agreement with the vortex locations and sink strengths measured in the smoke visualization experiment.

ACKNOWLEDGEMENTS

The author would like to thank the following people for their support during the completion of this work: Dr. Dick Desautel for agreeing to sit on my committee at the last moment; Dr. Thomas Pulliam for all his support with INS2D; Dr. Karlin Roth for her continuous comments and help (including a few of her Cray hours!); and finally, Dr. Nikos Mourtos who started me on this journey and without whom I would have been able to complete my degree. Thanks to all of you, and to my family and friends who supported me.

NOMENCLATURE

English Symbols

c	chord length (m)
c_l	lift coefficient
c_d	drag coefficient
c_m	moment coefficient
LE	leading edge
m	sink strength (m^3/s)
M	dimensionless sink strength
p	pressure (Pa)
Re	Reynolds number
s	span (m)
u, v	normal velocity components (m/s)
U_∞	Freestream velocity (m/s)
t	time (s)
V	velocity (m/s)
V_{sink}	velocity due to the sink (m/s)
x	sink distance downstream of the leading edge (mm)

X	dimensionless x-coordinate
y	sink distance above the plate (mm)
Y	dimensionless y-coordinate

Greek Symbols

α	angle of attack (degrees)
Γ	dimensionless vortex strength
ρ	density (kg/m ³)
τ	shear stress (Pa)
ν	dynamic viscosity (s/m ²)

Subscripts

inf	freestream conditions
min	minimum
max	maximum
v	viscous flux term

Superscripts

~	non-dimensional form
---	----------------------

TABLE OF CONTENTS

1. INTRODUCTION	1
1.1 MOTIVATION.....	1
1.2 PRESENT APPROACH.....	1
2. THE ANALYTICAL MODEL	3
2.1 PREVIOUS WORK.....	3
2.2 CURRENT RESEARCH.....	3
2.3 RESULTS.....	5
3. SMOKE FLOW VISUALIZATION	6
3.1 PREVIOUS WORK.....	6
3.2 CURRENT RESEARCH.....	7
3.3 APPARATUS.....	7
3.3.1 <i>Wind Tunnel</i>	7
3.3.2 <i>Test Model</i>	8
3.3.3 <i>Suction</i>	9
3.3.4 <i>Tunnel Velocity</i>	9
3.4 TWO- VERSUS THREE-DIMENSIONAL FLOW CONSIDERATIONS.....	9
3.5 PROCEDURE.....	10
3.6 DATA REDUCTION.....	11
3.6.1 <i>Smoke Tunnel Results</i>	11
3.6.2 <i>Dimensionless Parameters</i>	12
3.6.3 <i>Uncertainties</i>	12
3.7 RESULTS.....	13
3.7.1 <i>Vortex Formation</i>	13

3.7.2	<i>Location of Stable Vortices</i>	18
3.7.3	<i>Sink and Vortex Strengths</i>	20
3.7.4	<i>Trends in Vortex Formation</i>	22
3.7.5	<i>Reynolds Number and Sink Strength of Stable Vortices</i>	29
3.7.6	<i>Lift and Drag</i>	30
3.8	CONCLUSIONS	30
4.	NUMERICAL ANALYSIS	33
4.1	INTRODUCTION.....	33
4.2	PREVIOUS WORK.....	33
4.3	THE CODE INS2D.....	33
4.4	THE GOVERNING EQUATIONS.....	34
4.5	THE MESH	35
4.6	BOUNDARY CONDITIONS.....	38
4.6.1	<i>Boundary Conditions Supplied to INS2D</i>	38
4.6.2	<i>The Plate</i>	39
4.6.3	<i>The Freestream</i>	39
4.6.4	<i>The Sink</i>	40
4.6.5	<i>The Wake</i>	41
4.6.6	<i>Turbulence Modeling</i>	41
4.7	PROCEDURE.....	42
4.8	RESULTS.....	42
4.8.1	<i>Locating a Stable Vortex</i>	42
4.8.2	<i>Reynolds Number Effects</i>	46
4.8.3	<i>Vortex Dependence on Angle of Attack</i>	49
4.8.4	<i>Vortex Flows at Varying Downstream Stations</i>	54

4.8.5	<i>Discrepancies</i>	57
4.8.6	<i>Flow Without the Sink</i>	58
4.9	CONCLUSIONS	60
5.	SUMMARY AND RECOMMENDATIONS	62
5.1	SMOKE FLOW VISUALIZATION	62
5.2	NUMERICAL ANALYSIS	62
	REFERENCES	64
	APPENDIX A - EXPERIMENTAL DATA	65
	APPENDIX B - FLOW INPUT FILE	69

LIST OF FIGURES

Figure 1: Predicted vortex/sink locations for two models.....	4
Figure 2: Diagram of the smoke tunnel.....	8
Figure 3: Re-attached flow pattern.....	14
Figure 4: Vortex flow.....	15
Figure 5: Vortex flow patterns with the sink fixed at $(X, Y) = (0.25, 0.19)$	16
Figure 6: Separated flow pattern.....	17
Figure 7: Experimental runs at $\alpha=10^\circ$	19
Figure 8: Experimental runs at $\alpha=15^\circ$	19
Figure 9: Experimental runs at $\alpha=20^\circ$	20
Figure 10: Sink strength comparison.....	21
Figure 11: Vertical range of vortex formation. Distance from the LE fixed at 0.33 chords. $\alpha = 10^\circ$	23
Figure 12: Vertical range of vortex formation. Distance from the LE fixed at 0.36 chords. $\alpha = 10^\circ$	24
Figure 13: Vertical range of vortex formation. Distance from the LE fixed at 0.30 chords. $\alpha = 15^\circ$	25
Figure 14: Vertical range of vortex formation. Distance from the LE fixed at 0.40 chords. $\alpha = 15^\circ$	26
Figure 15: Vertical range of vortex formation. Distance from the LE fixed at 0.45 chords. $\alpha = 15^\circ$	27
Figure 16: Vertical range fixed at 0.2 chords. $\alpha = 10^\circ$	28
Figure 17: Vertical range fixed at 0.2 chords. $\alpha = 15^\circ$	29
Figure 18: The complete mesh used by INS2D.....	37
Figure 19: A close-up of the mesh surrounding the NACA 0012 airfoil.....	37
Figure 20: Experimental vortex and computational vortices at $\alpha = 15^\circ$	45
Figure 21: Vortex flow patterns computed at different Reynolds numbers.....	47
Figure 22: Lift and drag coefficients vs. Re for $X = 0.30, Y = 0.17, M = 0.664$	48
Figure 23: Moment coefficient vs. Re for $X = 0.30, Y = 0.17, M = 0.664$	48
Figure 24: Vortex flow at 5° angle of attack.....	50

Figure 25: Vortex flow at 10° angle of attack	50
Figure 26: Vortex flow at 15° angle of attack	51
Figure 27: Vortex flow at 20° angle of attack	51
Figure 28: Lift and drag coefficients at varying angles of attack	52
Figure 29: Moment coefficient at varying angles of attack.....	52
Figure 30: Lift and drag coefficients at various distances from the LE.	54
Figure 31: Moment coefficient at various distances from the LE.	54
Figure 32: Vortex flow at four separate horizontal distances from the LE of the airfoil	56
Figure 33: Unsteady flow at $\alpha = 15^\circ$, $M = 0.664$, $Re = 25\ 200$, $(X, Y) = (0.30, 0.17)$	59

LIST OF TABLES

Table 1: Uncertainties	13
Table 2: INS2D's Boundary Conditions Input File (BCMAIN.DAT)	38
Table 3: INS2D Boundary Conditions	39
Table 4: Reynolds Number Dependence of Vortex Formation	46
Table 5: Physical Constants	65
Table 6: Raw and Reduced Data	65
Table 7: INS2D's Flow Input File (AF.IN)	69

1. INTRODUCTION

1.1 Motivation

At high angles of attack it is increasingly difficult to prevent flow separation and loss of lift over airfoils. For example, fighter aircraft performing high angle of attack maneuvers present a unique challenge in maintaining steady flow over their wings. Also, aircraft require high lift coefficients at lower angles of attack typical of takeoff and landing. A possible solution to both of these problems is to trap a vortex over the wing, whether at low or high angle of attack¹. This work was undertaken in an attempt to verify and expand upon an analytical model for such a flow². Mourtos proposed that the presence of an artificial sink could generate a stable vortex over a plate similar in nature to the leading edge vortex generated by the leading edge of a delta wing at high angle of attack. The results of this analytical work generated sufficient interest in examining the proposed flow both experimentally and computationally, leading to a smoke flow visualization experiment and then to computational modeling in INS2D³⁻⁵.

1.2 Present Approach

The objective of this work was to check both experimentally and computationally the results of Mourtos and Brooks². This was accomplished in two ways:

1. A smoke visualization test was performed to observe the vortex flow over a flat plate. Fluid was removed in the spanwise direction using suction.

2. A numerical model of the flow was run using INS2D.

2. THE ANALYTICAL MODEL

It is not the purpose of this paper to detail the analytical model of Mourtos and Brooks². However, since the experiment was designed with testing those results, a brief discussion of the analytical model will be presented.

2.1 Previous Work

The first analytical attempts to predict a stable vortex over an airfoil were made in 1977 by Saffman and Sheffield¹. Saffman and Sheffield considered steady, two-dimensional, inviscid, incompressible flow over a flat plate, without suction. By using conformal mapping, they were able to predict stable vortex loci for certain angles of attack. However, Saffman and Sheffield were unable to satisfy the Kutta condition at the leading edge. Huang and Chow⁶ expanded this work by using the same technique to analyze the flow over a Joukowski airfoil. V. J. Rossow⁷ followed by adding both a leading edge flap and a sink at the vortex core. Rossow's work generated many vortices, but the stability of these vortices was considered questionable.

2.2 Current Research

The analytical work performed by Mourtos² is an extension of the work of Saffman and Sheffield¹. Their model consisted of a single vortex freestanding over a flat plate. They found no unique solution for the location of the vortex. Instead, a family of vortex locations was generated for each angle of attack where the vortex strength increased with distance from the plate (Figure 1).

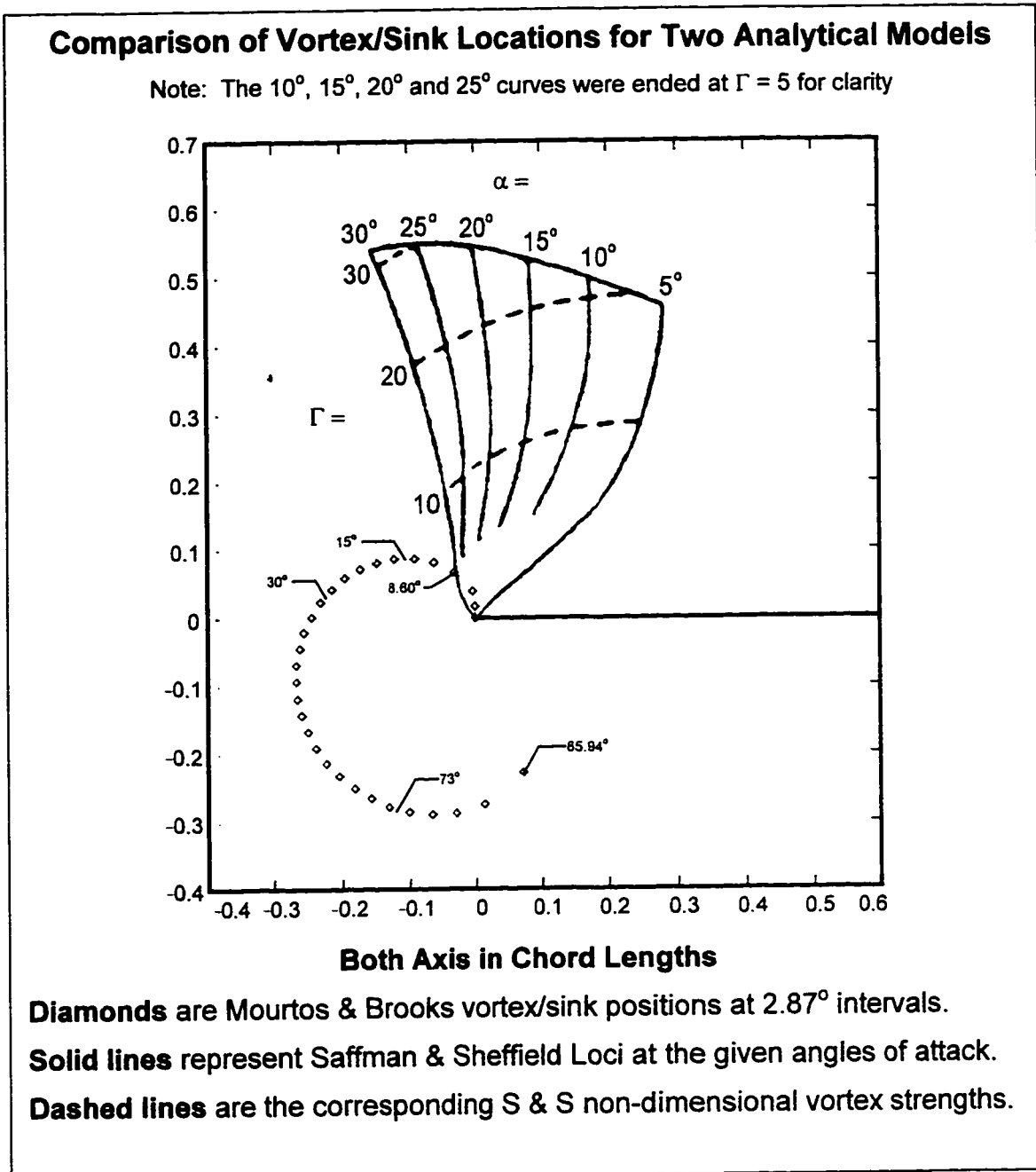


Figure 1: Predicted vortex/sink locations for two models

The two major changes to the model were:

1. A sink was added at the location of the free vortex to satisfy the Kutta condition at both the leading and trailing edges.

1. A sink was added at the location of the free vortex to satisfy the Kutta condition at both the leading and trailing edges.
2. To generate a unique vortex/sink location at a specified angle of attack, a constraint was added to require the total force on the plate to be perpendicular to the plate.

With the addition of the above items, it can be shown² that a unique solution for the vortex/sink combination exists for a given angle of attack that satisfies the Kutta condition at both the leading and trailing edges.

2.3 Results

The model above was modified and solved uniquely for the free and bound vortex strengths, their positions above (or in some cases below) the plate, and sink strength. The vortex/sink position moves in a counterclockwise fashion starting from the leading edge all the way around and below the plate. An interesting comparison can be made between the results of Mourtos and Brooks and Saffman and Sheffield in Figure 1. Notice that at low angles of attack the vortex positions are in the same general area, above and slightly ahead of the leading edge of the plate. Dimensionless vortex strength is also comparable at low angles of attack. At high angles of attack Saffman and Sheffield did not give any data; however, the trend of vortex locations are similar to Mourtos and Brooks.

3. SMOKE FLOW VISUALIZATION

3.1 Previous Work

Vortices can be formed from shear layers. Shear layers are comprised of small-scale vortices ranging in magnitude up to the thickness of the shear layer itself. These vortices are small in strength, and dissipate with the effects of viscosity. A detached shear layer can be used to increase the vorticity of the flow around it. The shear layer created when a boundary layer encounters the edge of a backward facing step is one such method of accomplishing this. The velocity differential between the moving shear layer and the stagnant flow behind the step causes a large increase in vorticity of the stagnant fluid. It is possible to cause the formation of a single, large vortex, using suction or other means. Riddle⁸ used suction in two-dimensional water tunnel tests demonstrating that a single vortex could be maintained at some sink rates for a limited range of vertical sink locations. In these cases, the trapped vortex created by the detached shear layer were no more than 10% higher than the height of the step. This caused little appreciable acceleration in the flow over the step, and the chance for increased lift of a corresponding airfoil of this type was equally small. Rossow⁷ performed a similar water tunnel experiment with likewise results. Rossow also tried some preliminary wind tunnel experiments using flaps on the upper surface of the airfoil to help contain the vortex in addition to the presence of suction⁷. These experiments showed that it was possible to contain a trapped vortex over the surface of the airfoil.

3.2 Current Research

The current work that has been performed at the San Jose State University smoke tunnel was designed to meet the following goals: generate a stable vortex over a flat plate at an angle of attack through the use of suction and compare the vortex/sink locations to the analytical work of Mourtos and Brooks².

3.3 Apparatus

3.3.1 Wind Tunnel

The wind tunnel used in this experiment was the 3 ft x 3 ft x 2.5 in smoke tunnel in the aerodynamics laboratory of the Aerospace Engineering Department at San Jose State University. The tunnel has a minimum freestream velocity of 1 m/s and a maximum freestream velocity of 8 m/s. These velocities corresponded to freestream Reynolds numbers based on the chord of the airfoil of 8400 and 67,200 respectively.

Smokelines were generated every inch vertically along the central horizontal streamlines. The smoke was illuminated with two fluorescent lights along the top and bottom of the tunnel.

One permanent hole was already in place on the back side of the test section limiting the aperture of the two orifices to an inner diameter of 3/8 in. Abiding by this restriction, the maximum aperture size of 3/8 in was chosen for two reasons: it was large enough to permit sufficient fluid removal rates (given the strength of the vacuum pumps available), and small enough (less than 10%

of the chord length) to reasonably simulate a point sink. A diagram of the smoke tunnel used is shown in Figure 2.

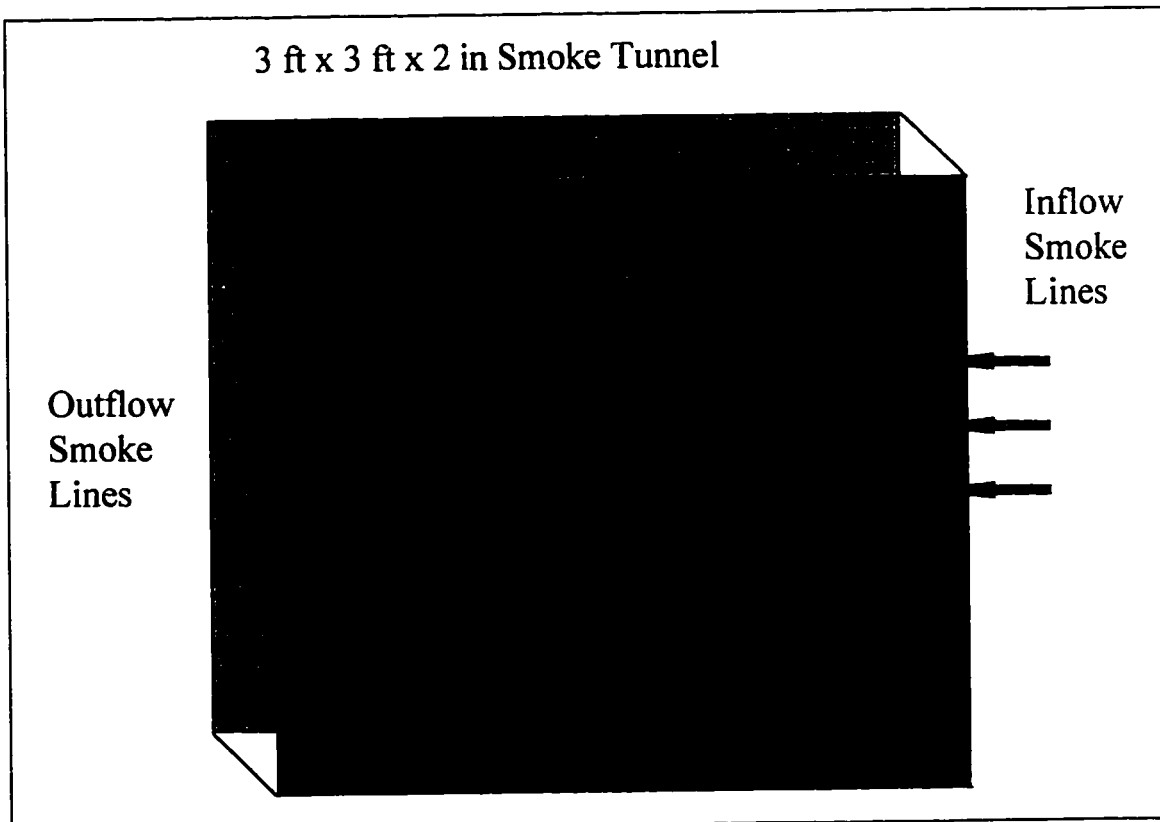


Figure 2: Diagram of the smoke tunnel

3.3.2 Test Model

The test model was a 4 in long by 2.5 in wide by 1/16 in thick brass plate attached to a sting mounted on the trailing edge of the plate. The trailing edge was chosen rather than the underside of the plate, because vortices were predicted to form on the underside of the plate, and any intrusion to the flow at that point would likely disrupt vortex formation. The plate stretched completely across the width of the tunnel to simulate a two-dimensional flow.

3.3.3 Suction

Suction was provided through two stationary orifices in the test section of the tunnel from two vacuum cleaners rated at a minimum of 1.5 hp. Each vacuum cleaner removed fluid from one orifice. The volumetric flow rate was measured and controlled through each orifice using separate flow meters and valves. The maximum amount of suction was 6 ft³/min through each orifice for a total of 12 ft³/min. All trials ran with identical suction rates through each orifice.

3.3.4 Tunnel Velocity

The freestream velocity of the smoke tunnel was calibrated with a pitot tube. Using the pitot tube measurements, the mechanical axis of the shutter used to control airspeed was marked in m/s. Once calibrated, the pitot tube was removed and airspeed readings were taken directly from the mechanical axis. After the testing, the pitot tube was used to check the calibration of the tunnel to within 0.25 m/s.

3.4 Two- versus Three-dimensional Flow Considerations

Suction provided by the two orifices on opposite sides of the test section removed fluid from the flow. Any fluid traveling between the stagnation streamlines (one on the lower and one on the upper surface of the plate) is removed by the suction through the orifices. This generates a three-dimensional flow. For vortices that formed with the sink located at their core, testing showed this three-dimensional flow to be confined to the core of the vortex. The smoke

lines of primary interest to us remained two-dimensional. Only at the core of the vortex did the smoke lines break up and disperse to be evacuated through the orifices. This was aided by providing identical suction rates at both orifices. If the rates were slightly different, the vortex exhibited a three-dimensional nature as the smoke lines were pulled to one side and spiraled into the stronger sink.

Three-dimensional effects did become apparent when the sink was placed near the surface of the plate. The flow condition that resulted when the sink was placed too close to the surface of the plate showed a three-dimensional structure that eludes two-dimensional analysis. This flow can be seen in Figure 3, and was termed re-attached flow. As shown in the figure, the flow separates over the leading edge of the plate and re-attaches itself downstream of the sink location. The small separation bubble that is produced at the leading edge may contain a small and weak vortex, which is not centered at the location of the sink. In our two-dimensional flow analysis, only vortices centered at the sink were considered. Although this flow pattern was of no interest for the purposes of this paper, a separate investigation of this flow is recommended in section 5.

3.5 Procedure

Tests were run in the following manner. The model was placed at the predetermined angle of attack and positioned at a specific location underneath (or above) the sink. The smoke was turned on and the flow rate set at the minimum possible value of 1 m/s without suction. Suction was then applied at

the highest rate possible, 12 ft³/min. The tunnel freestream velocity was then increased slowly to the tunnel maximum of 8 m/s. Tunnel velocities were recorded when changes in the flow pattern were observed, such as vortex formation and breakdown. A small number of tests were filmed using a camcorder; however, the majority of the tests were not filmed.

Tests were directed to determine where the stable vortices might be found. The majority of the tests were at angles of attack of 10°, 15°, 20°, and 25° to limit the amount of testing required.

3.6 Data Reduction

3.6.1 *Smoke Tunnel Results*

The complete table of raw and reduced results is presented in appendix A. Tunnel velocity could not be lowered below 1 m/s or raised above 8 m/s. Values of 1 m/s or 8 m/s (corresponding to Re values of 8400 and 67 200) in the raw data *do not* indicate that the flow pattern being described began or terminated at the stated speed. Instead values of 1 m/s or 8 m/s indicate that the flow pattern was present at the stated velocity.

In all cases re-attached flow was observed below the minimum range recorded for stable vortex flow. Also in all cases, separated flow was observed above the maximum velocity range recorded for stable vortex flow. No exceptions were observed.

3.6.2 Dimensionless Parameters

In order to make the large amount of data gathered more tractable for analysis and presentation, the following dimensionless parameters were introduced:

The dimensionless sink strength

$$M = \frac{m}{V_{\infty} c} \quad (3.1)$$

The dimensionless x coordinate (specified positive downstream of the LE)

$$X = \frac{x}{c} \quad (3.2)$$

The dimensionless y coordinate (specified positive above the plate)

$$Y = \frac{y}{c} \quad (3.3)$$

Through the use of the dimensionless parameters above and the angle of attack, the data was reduced to four variables (with the dimensionless sink strength specified for each change in the flow pattern). Even though the velocity of the tunnel was the only variable modified during an actual tunnel test, this was equivalent to modifying the dimensionless sink strength. Therefore, from here on, all discussions will refer to the dimensionless sink strength instead of the dimensional velocity associated with the onset or disappearance of a flow pattern.

3.6.3 Uncertainties

Uncertainties for all of the physical parameters measured during testing are listed in table 1 below. The most significant source of error was the 0.25 m/s

uncertainty in the freestream velocity. This resulted in a high (24%) uncertainty for the Reynolds number.

Table 1: *Uncertainties*

Variable	Uncertainty	Cause
V	± 0.25 m/s	Variability in Pitot tube measurements, see section 6.3.4
m	± 0.5 ft ³ /s (0.014 m ³ /s)	Accuracy of measuring device
c	± 1 mm	Accuracy of measuring device
x	± 1 mm	Accuracy of measuring device
y	± 1 mm	Accuracy of measuring device
X	± 0.01	Derived from x uncertainty above
Y	± 0.01	Derived from y uncertainty above
α	$\pm 2^\circ$	Maximum difference between before and after angle of attack measurements
ν	± 0.1 m ² /s	Approximation of conditions taken from standard atmospheric table
Re	$\pm 24\%$ @ V = 1 m/s $\pm 17\%$ @ V = 4 m/s	Calculated from ν , c, and V uncertainties

3.7 Results

3.7.1 Vortex Formation

The first tests performed were attempts to verify the analytical model of Mourtos and Brooks². Several angles of attack were tried: 11.5°, 31.5°, and 60.0°. No vortices were observed to form in the locations predicted analytically regardless of the sink strength. However, stable vortices did form at locations other than those predicted by theory.

Stable vortex formation was observed from 5° angle of attack, up to 40° angle of attack. At angles greater than 40°, no vortices were observed, but

detailed testing was not performed and vortex formation should not be ruled out, especially if larger sink strengths are used. A complete investigation of possible vortex formation past 25° was not performed. Instead, the effort was focused on four angles of attack: 10° , 15° , 20° and 25° .

To aid in the visualization of the flow, six still frames were captured from actual tests. These frames are shown in Figure 3 through Figure 6. Four distinct flow patterns were observed:

1. **Re-attached flow.** This flow pattern was observed for angles of attack less than 5° and for larger angles of attack where the sink strength was too high for vortex formation. The flow separated at the leading edge producing a small separation bubble, possibly enclosing a weak vortex. The flow re-attached itself downstream of the sink (Figure 3).

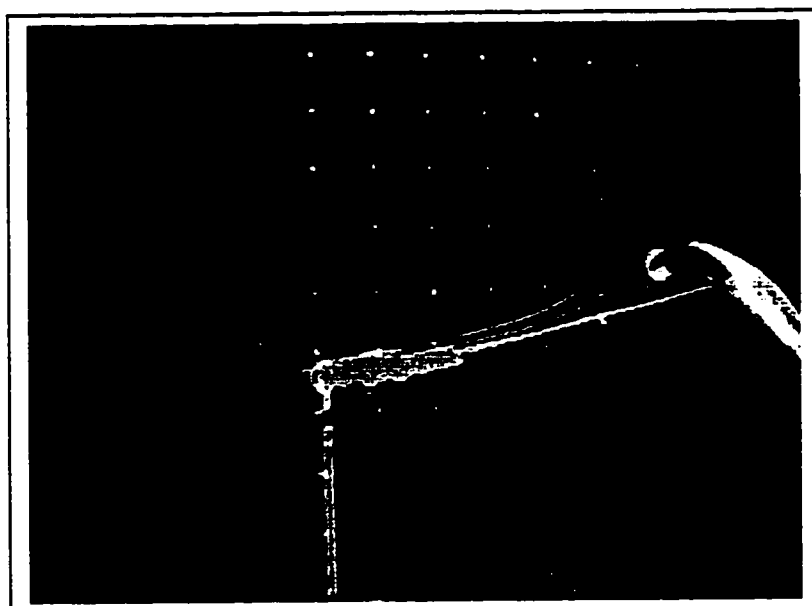


Figure 3: Re-attached flow pattern
 $\alpha = 10^\circ$, $(X, Y) = (0.19, 0.13)$, $M = 0.439$, $Re = 31612$, $V = 3.75$ m/s

2. **Stable vortex flow.** As the angle of attack increased to values equal to or larger than 5° the proper sink strengths caused flow separation from the leading edge to take the form of a vortex centered at the sink (Figure 4 and Figure 5). The flow again reattached downstream of the vortex/sink location. This is the flow pattern of greatest interest because of the high lift increments

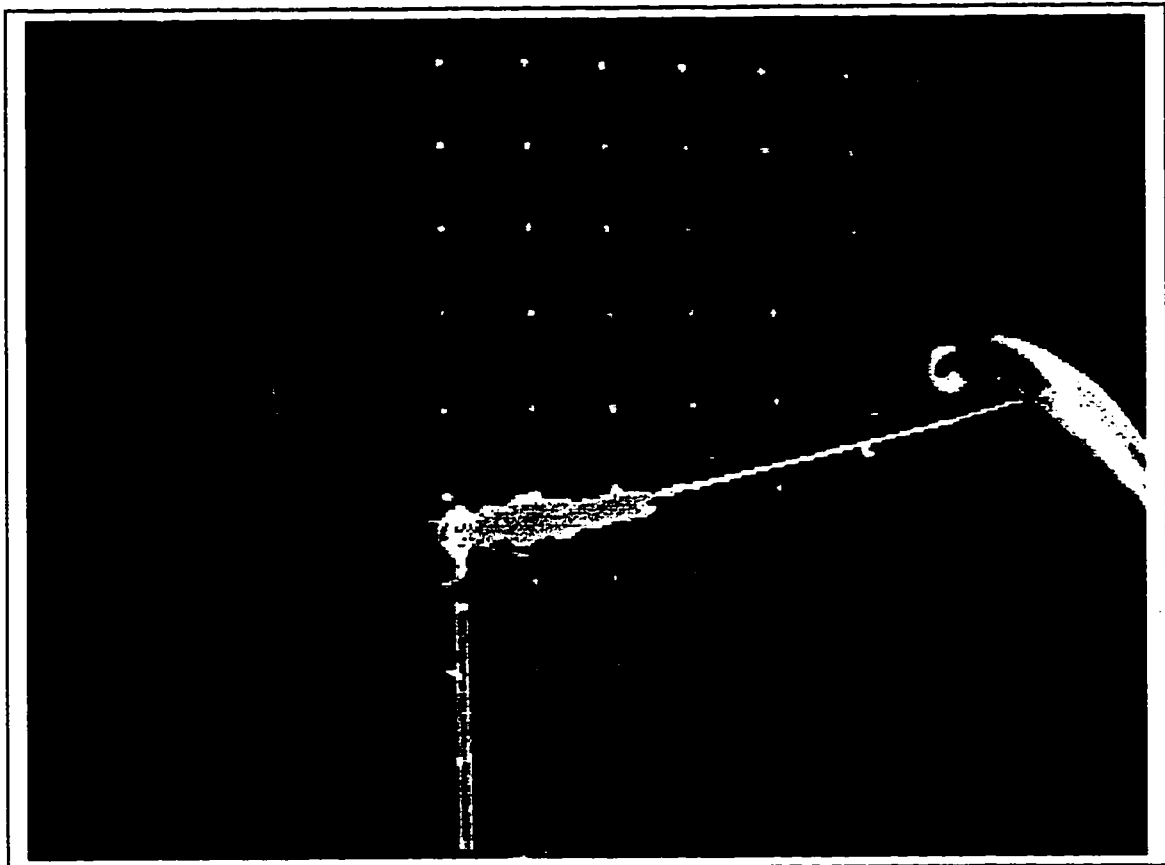
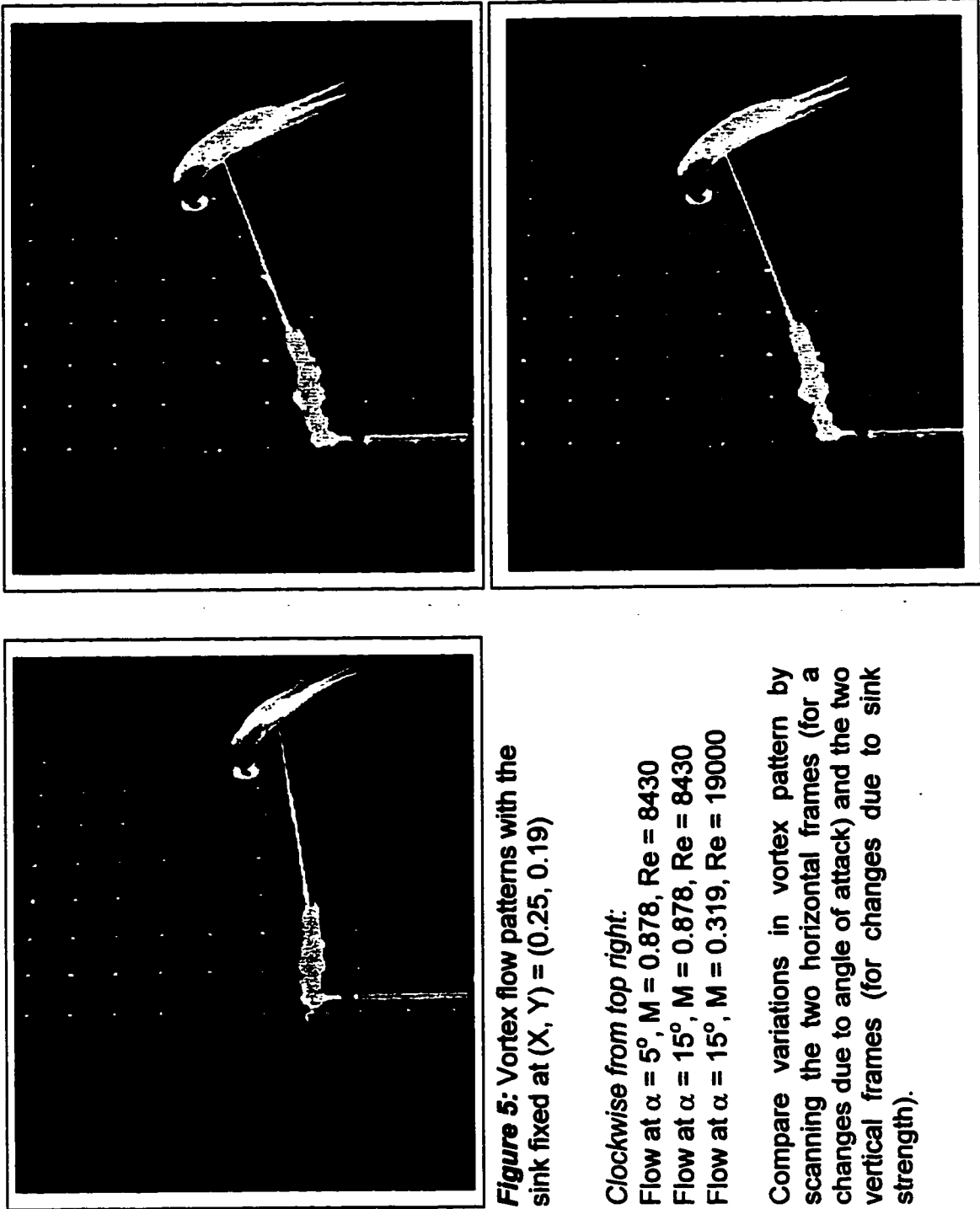


Figure 4: Vortex flow

$\alpha = 10^\circ$, $(X, Y) = (0.19, 0.13)$, $M = .234$, $Re = 16860$, $V = 2.0$



3. **Oscillatory flow.** For some combinations of angle of attack, sink strength and position, a vortex would form but then it would break down and travel downstream. A new vortex would form again on the plate and the whole process would be repeated.
4. **Fully separated flow.** This is the familiar flow studied by Helmholtz (Figure 6). There is no flow reattachment.

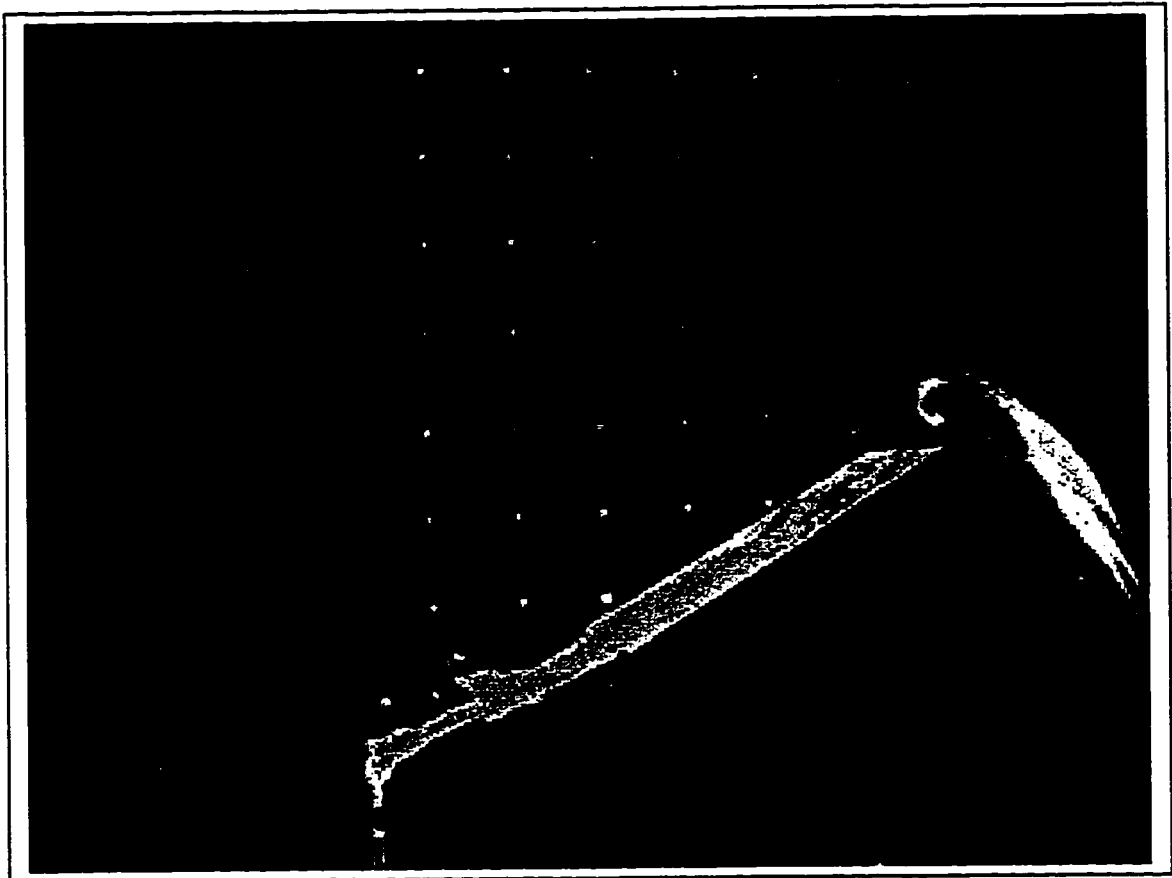


Figure 6: Separated flow pattern

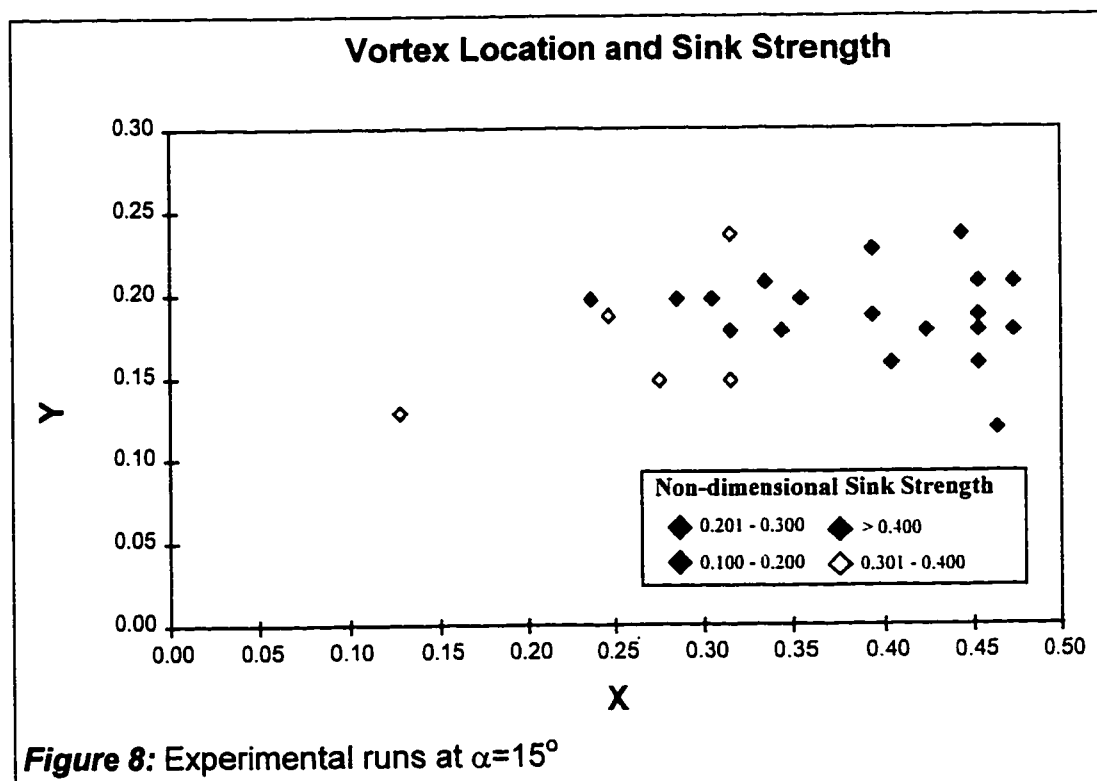
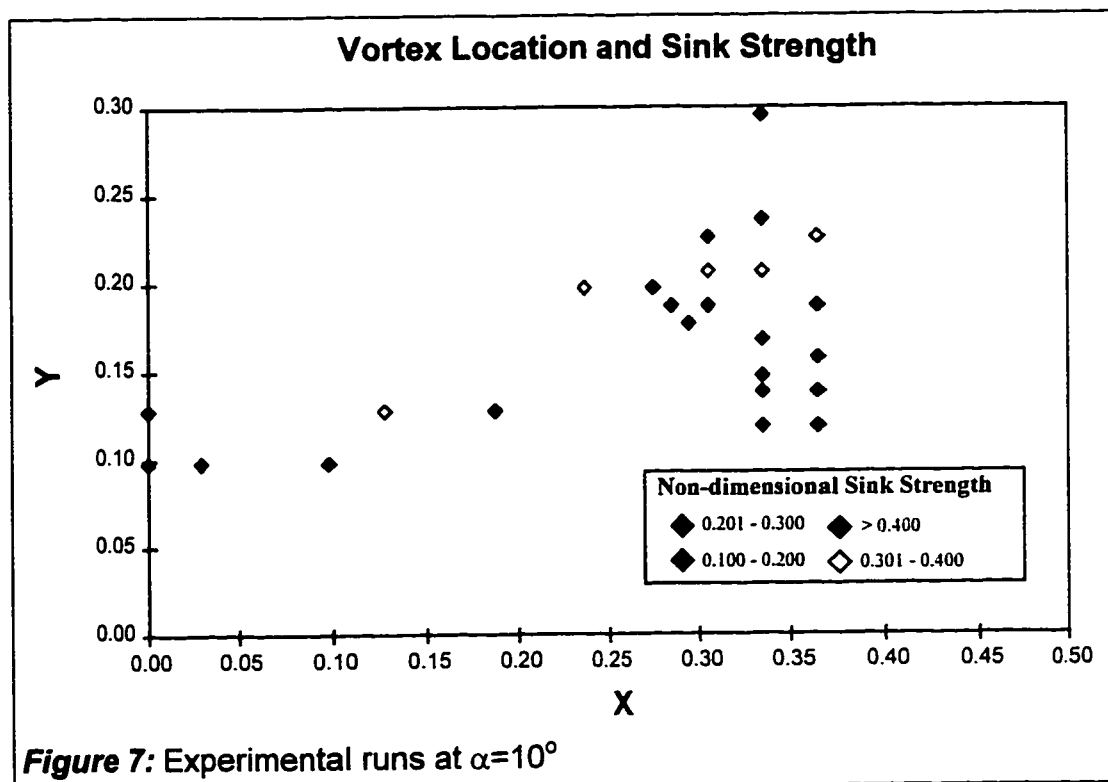
$\alpha = 27.5^\circ$, $(X, Y) = (0.03, 0.11)$, $M = 0.439$, $Re = 16860$, $V = 2$ m/s

By examining Figure 5, as the sink moved away from the plate, the vortex grew larger. Also, as the dimensionless sink strength was decreased, the vortex grows in size (until breakdown occurred).

3.7.2 Location of Stable Vortices

Stable vortices were found at angles of attack between 5° and 40° . These vortices were located between one third and one half a chord length downstream of the leading edge and from 0.1 to 0.3 chord lengths above the plate. Very small angles of attack (less than 5°) produced re-attached flow.

For the four angles of attack studied (10° , 15° , 20° , and 25°) three-dimensional contour plots were constructed for the dimensionless sink strength as a function of X and Y. These four plots (Figure 7-Figure 9) contain all of the data collected on the four variables. They are useful in observing the areas of vortex formation, and the locations of the lowest sink strengths. Data points were generally not taken below 0.1 chords above the plate as reattached flow or fully separated flow was usually observed in these cases (Figure 3 and Figure 6).



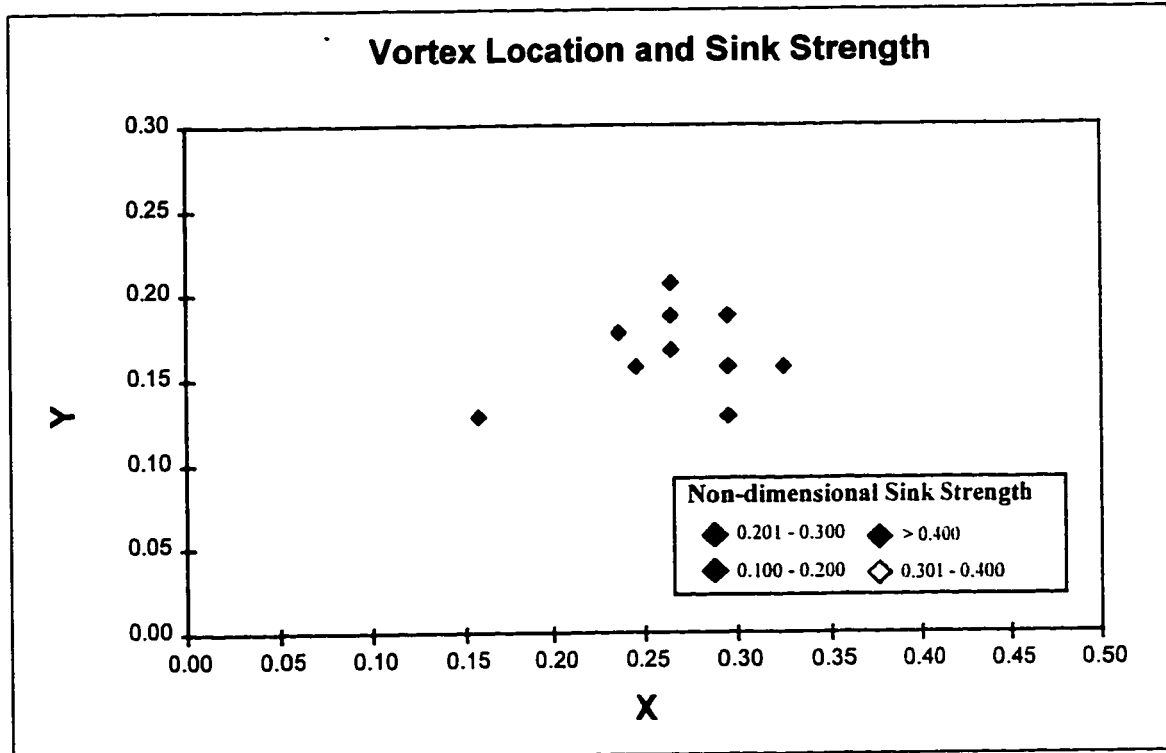


Figure 9: Experimental runs at $\alpha=20^\circ$

3.7.3 Sink and Vortex Strengths

While vortex strengths for the experimental and computational vortices were not obtained, the sink strengths in both cases were known. A comparison of the predicted analytical sink strengths and the minimum/maximum experimental and computational sink strengths is shown in Figure 10.

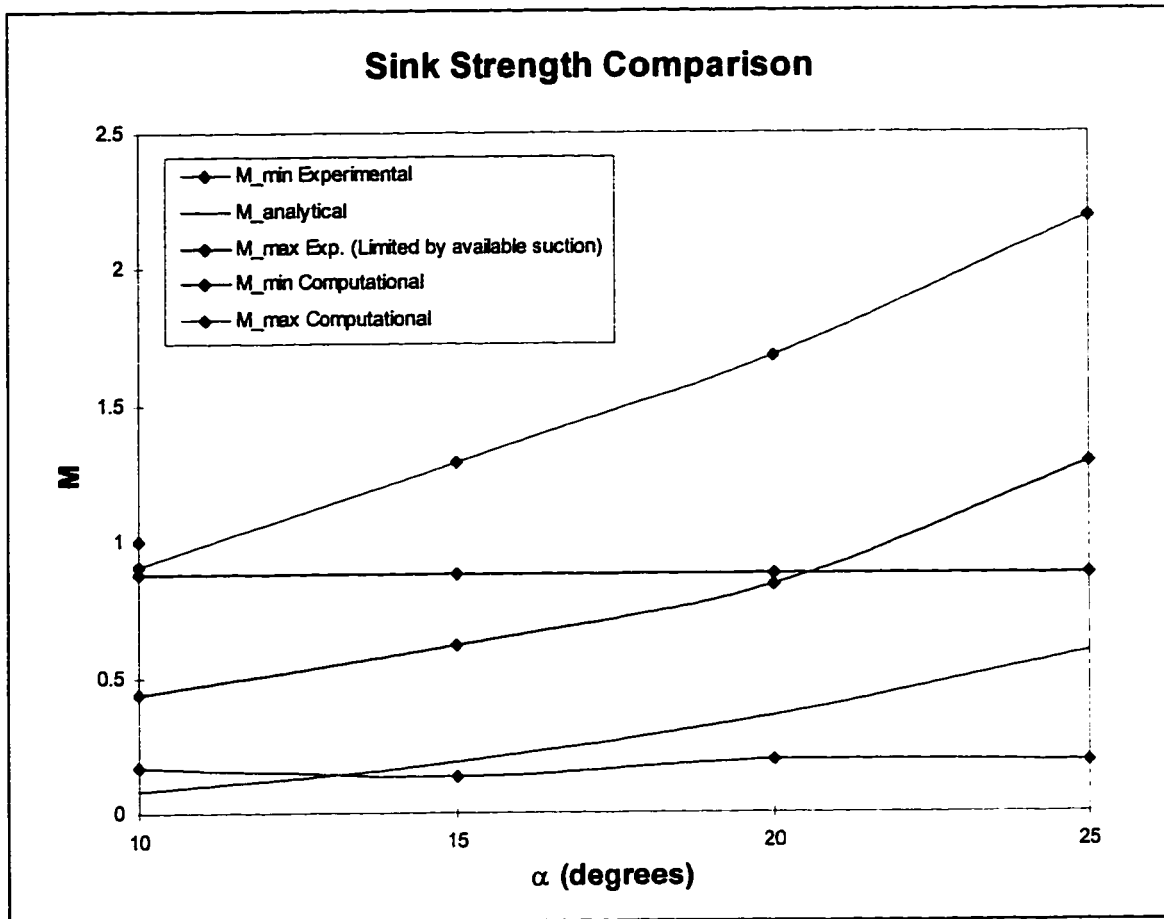


Figure 10: Sink strength comparison

The suction predicted by the analytical model was achieved at angles of attack between 15 and 25 degrees. At 10° angle of attack, the minimum sink strength required to generate a stable vortex was roughly double that predicted by the analytical model. Experimentally, there was a physical limit on the amount of suction that could be provided by the vacuums. This limited the maximum experimental non-dimensional sink strength to a value of 0.878. Figure 10 represents the minimum and maximum sink strengths found by *any* stable vortex generated at the given angle of attack. So it is possible that while certain regions

of sink strength overlap for both the experimental and computational trials, those overlapping values could be representative of sink strengths achieved at different vortex locations in both the computational and experimental analysis. An in depth analysis of this is presented in Section 4.8.1 where it was found that in some cases a computational vortex could be generated at the identical experimental conditions, though not in all cases.

3.7.4 Trends in Vortex Formation

Selected two-dimensional plots of the sink strength versus a single coordinate (either X or Y) were generated in an effort to trend the formation of the experimentally generated vortices. Each figure is separated into two or three flow patterns with re-attached flow occupying the upper left region of the graphs, vortex flow occupying the “bucket” formed by the curve or curves, and fully separated flow occupying the lower region of the figure. By examining Figure 11, we can see how the sink strength and vertical distance from the plate affected vortex formation at 0.33 chords downstream of the leading edge. As the sink was raised from the plate, the required suction maintaining the vortex grew. At 36% of the chord downstream we have a similar situation (Figure 12).

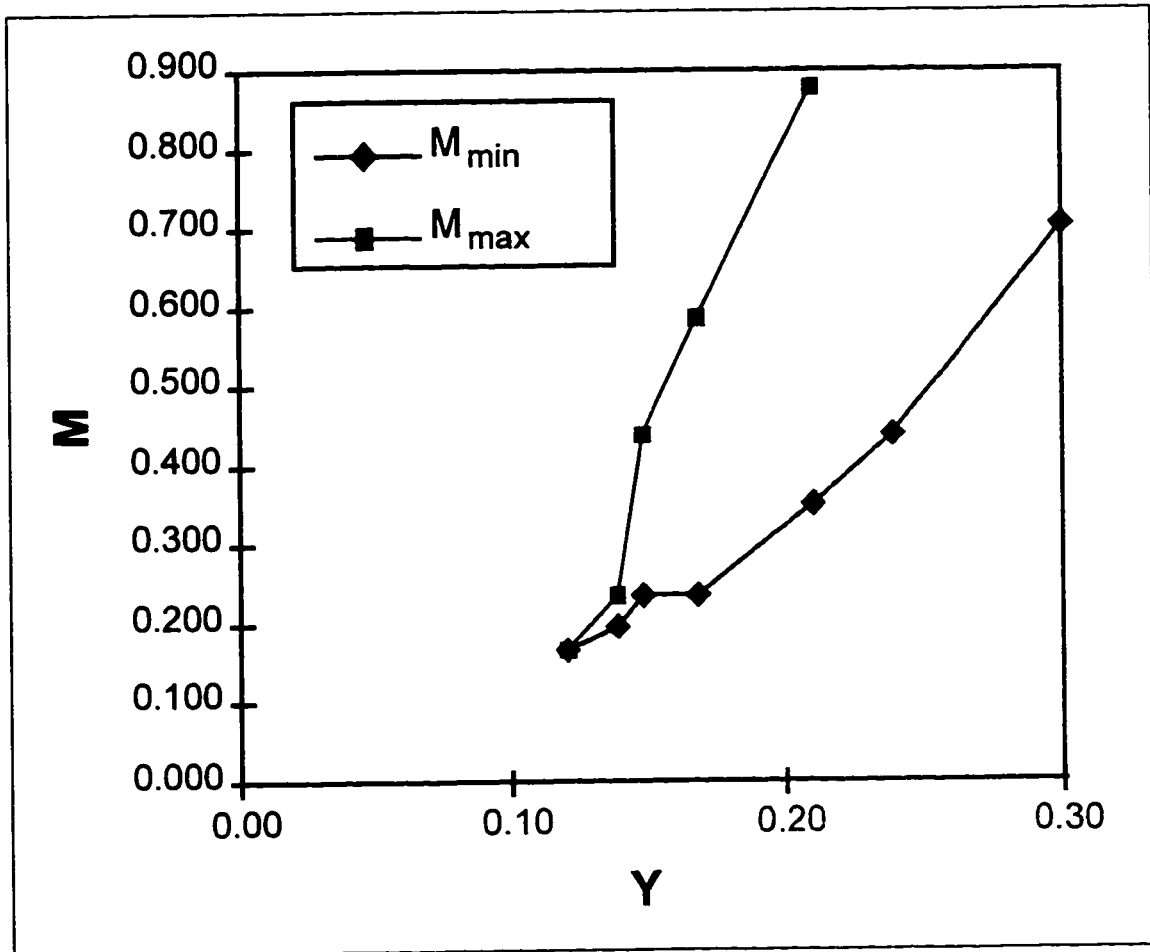


Figure 11: Vertical range of vortex formation. Distance from the LE fixed at 0.33 chords. $\alpha = 10^\circ$.

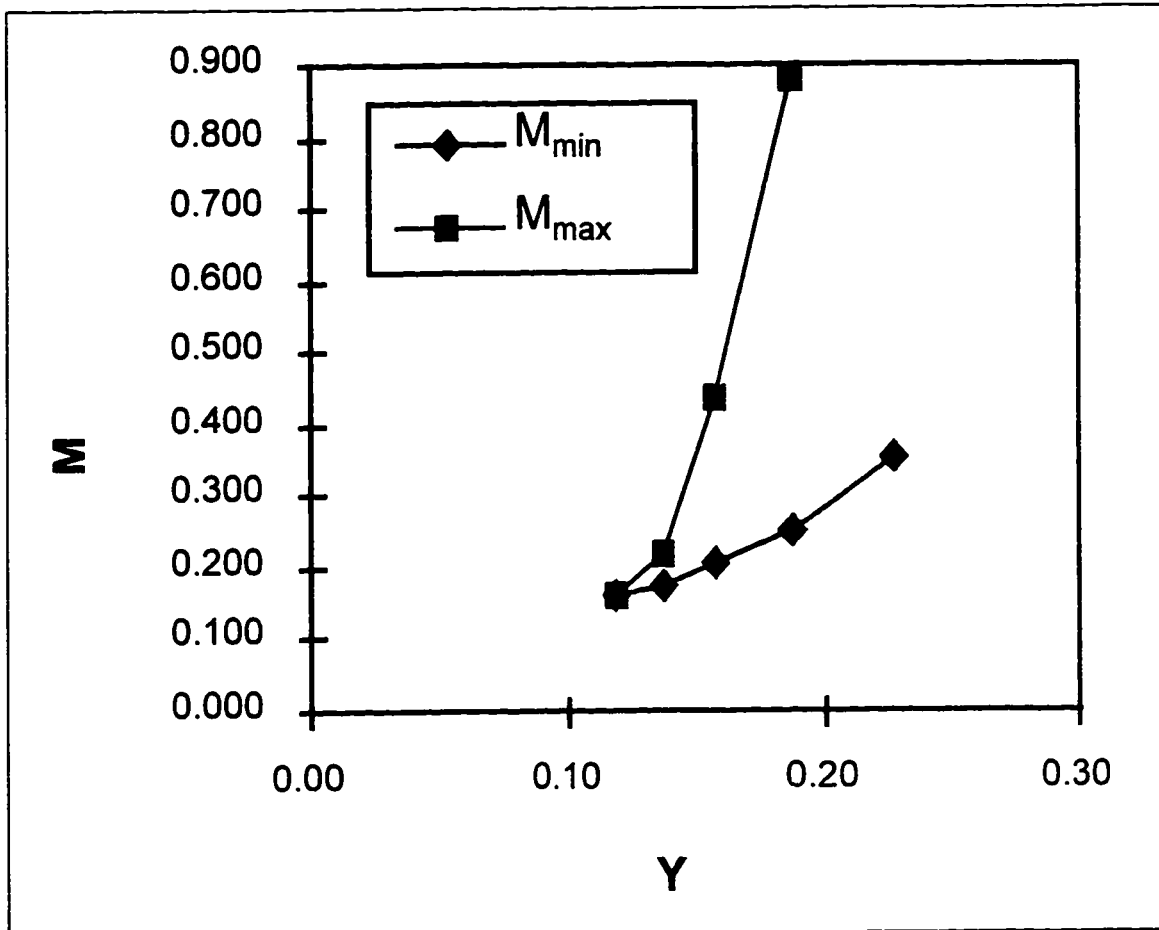


Figure 12: Vertical range of vortex formation. Distance from the LE fixed at 0.36 chords. $\alpha = 10^\circ$.

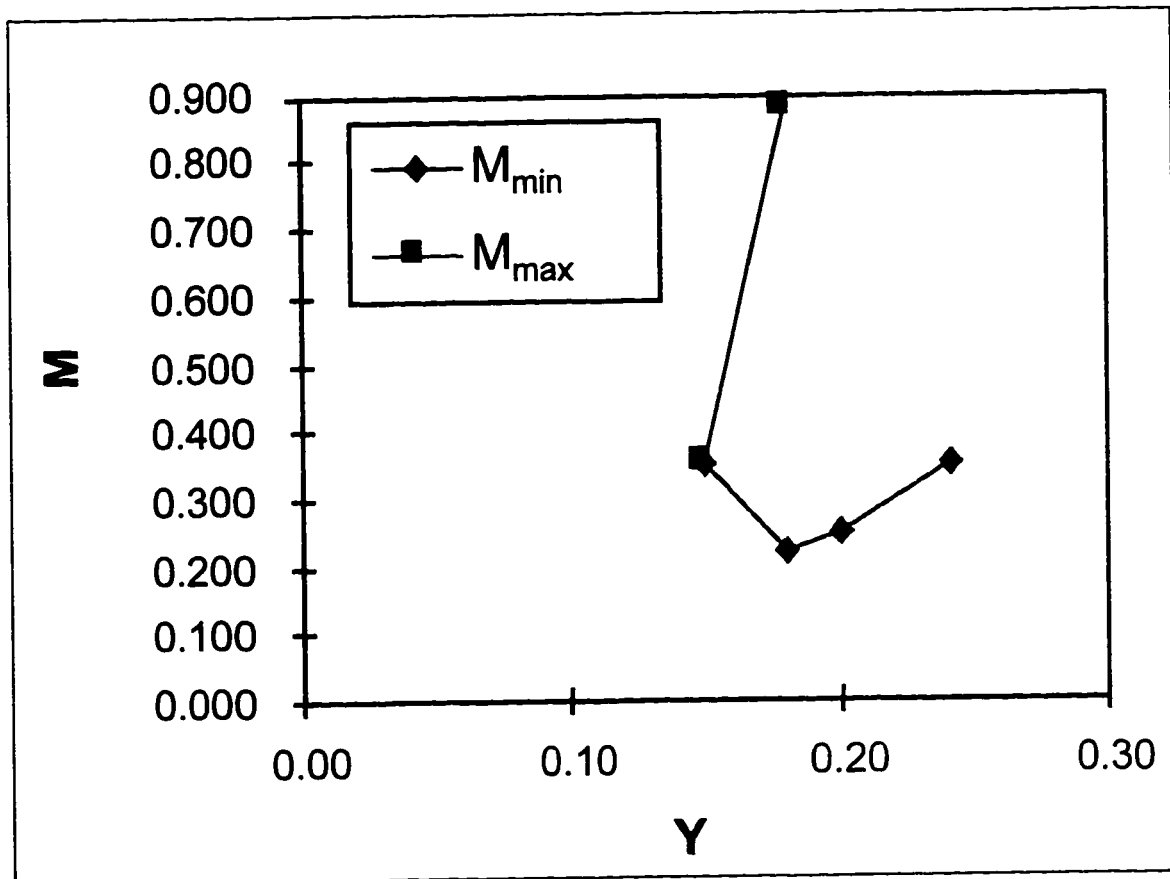


Figure 13: Vertical range of vortex formation. Distance from the LE fixed at 0.30 chords. $\alpha = 15^\circ$.

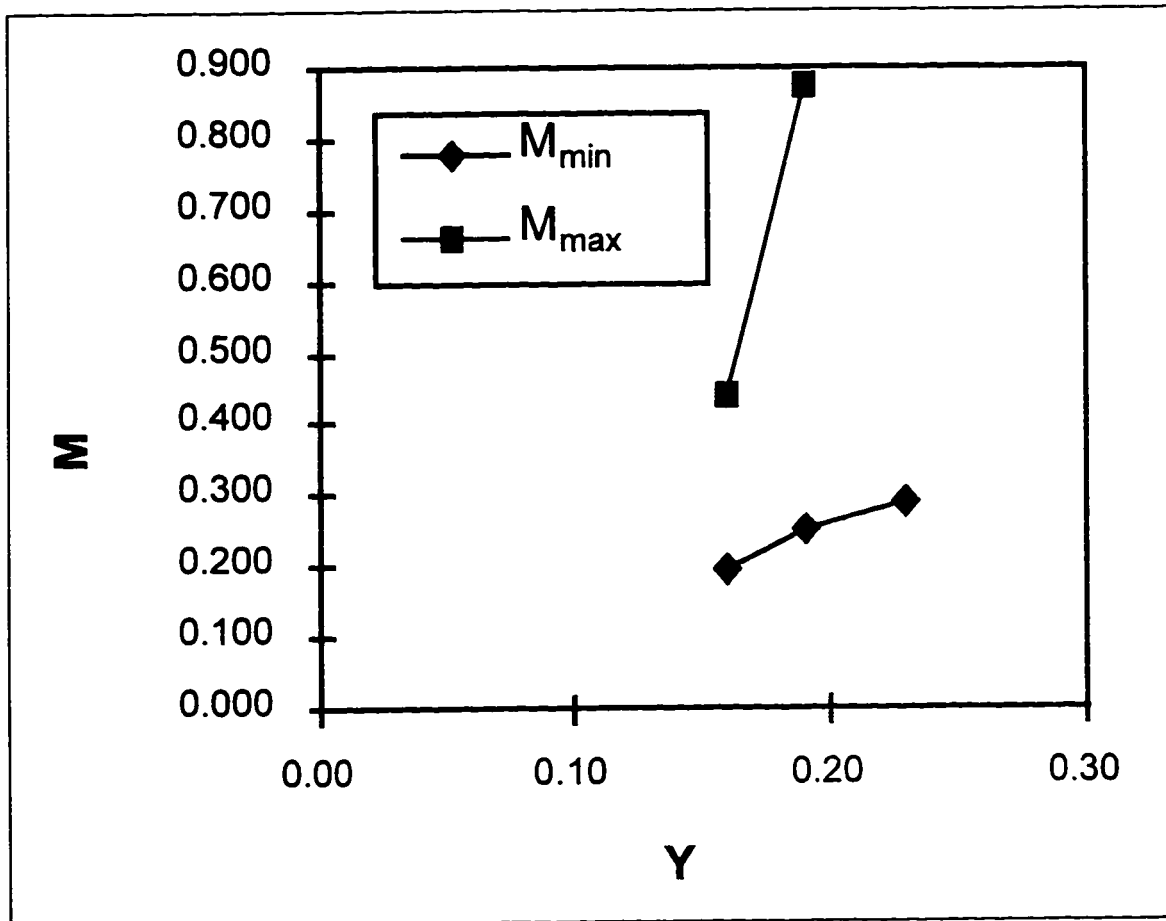


Figure 14: Vertical range of vortex formation. Distance from the LE fixed at 0.40 chords. $\alpha = 15^\circ$.

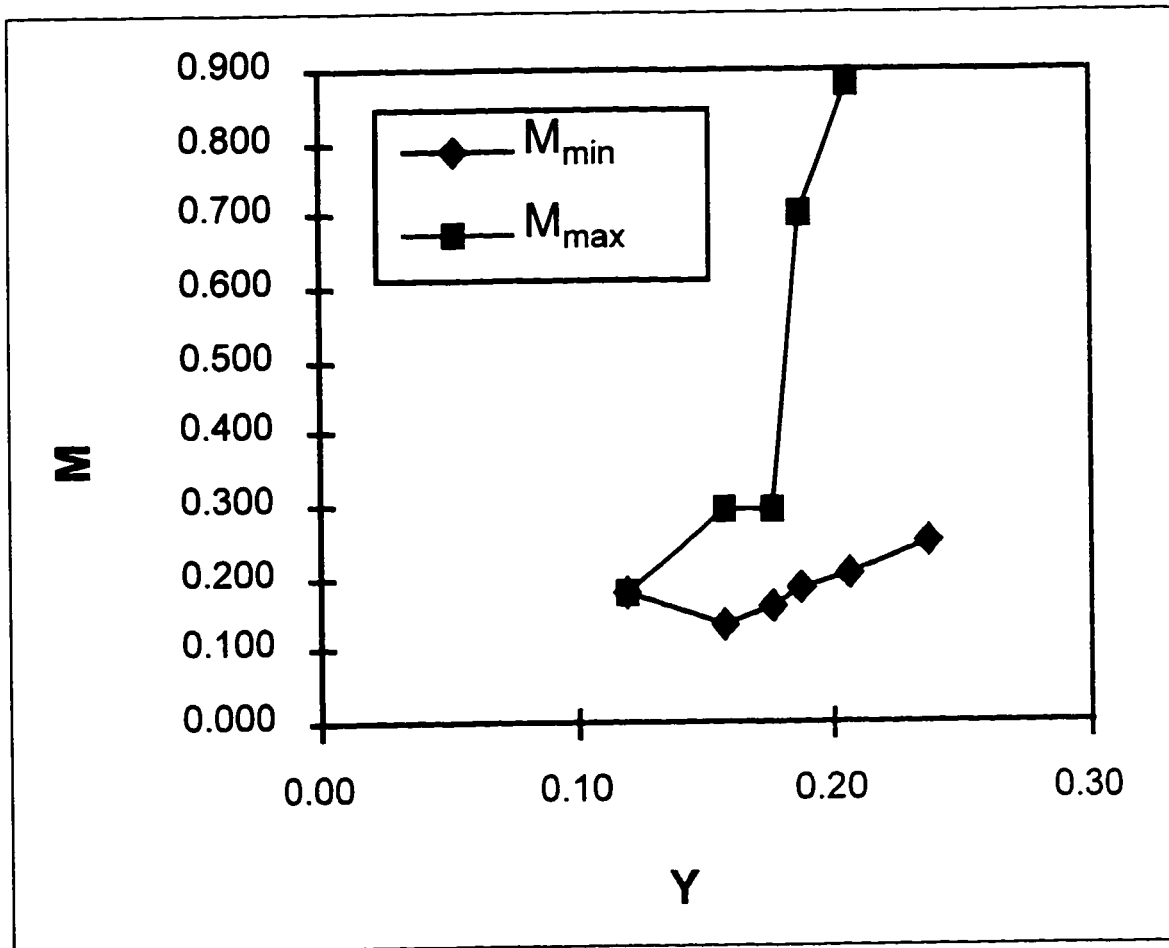


Figure 15: Vertical range of vortex formation. Distance from the LE fixed at 0.45 chords. $\alpha = 15^\circ$

However, for a larger angle of attack we observe a significant change in sink strengths and vertical distance from the plate for vortex formation (Figure 11-Figure 15). Notice how the “bucket” of stable vortices is largest at 45% of the chord. This can be compared with Figure 8 (a three-dimensional representation of the same data).

Horizontal placement of the sink was surprisingly arbitrary, from 0.1 chords downstream of the leading edge to a full half chord downstream of the leading edge. However, a definite band of low sink strength vortices was found

for each angle of attack. Two examples are shown for a vertical distance of 0.2 chords above the plate (Figure 16 and Figure 17). Notice the larger and lower bucket for $\alpha = 15^\circ$.

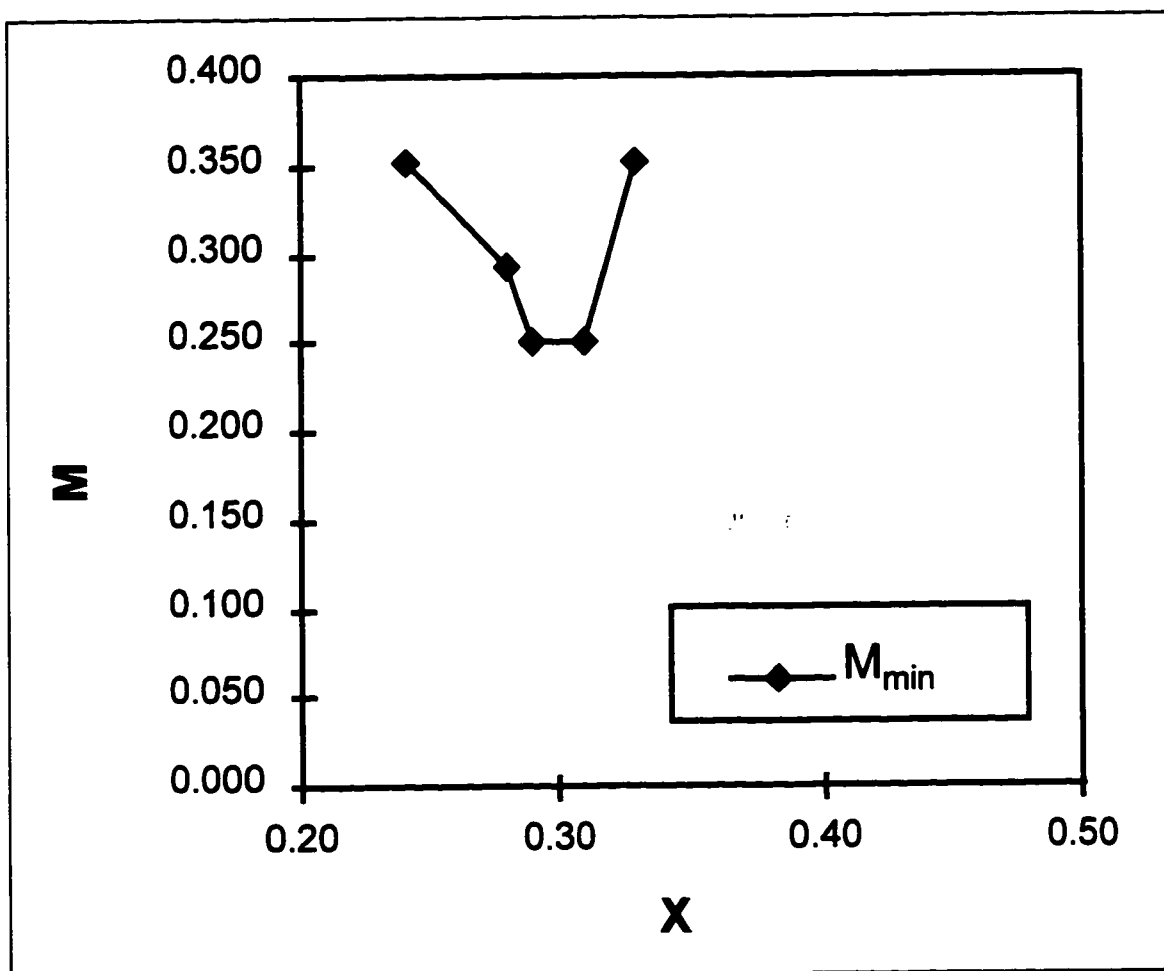


Figure 16: Vertical range fixed at 0.2 chords. $\alpha = 10^\circ$

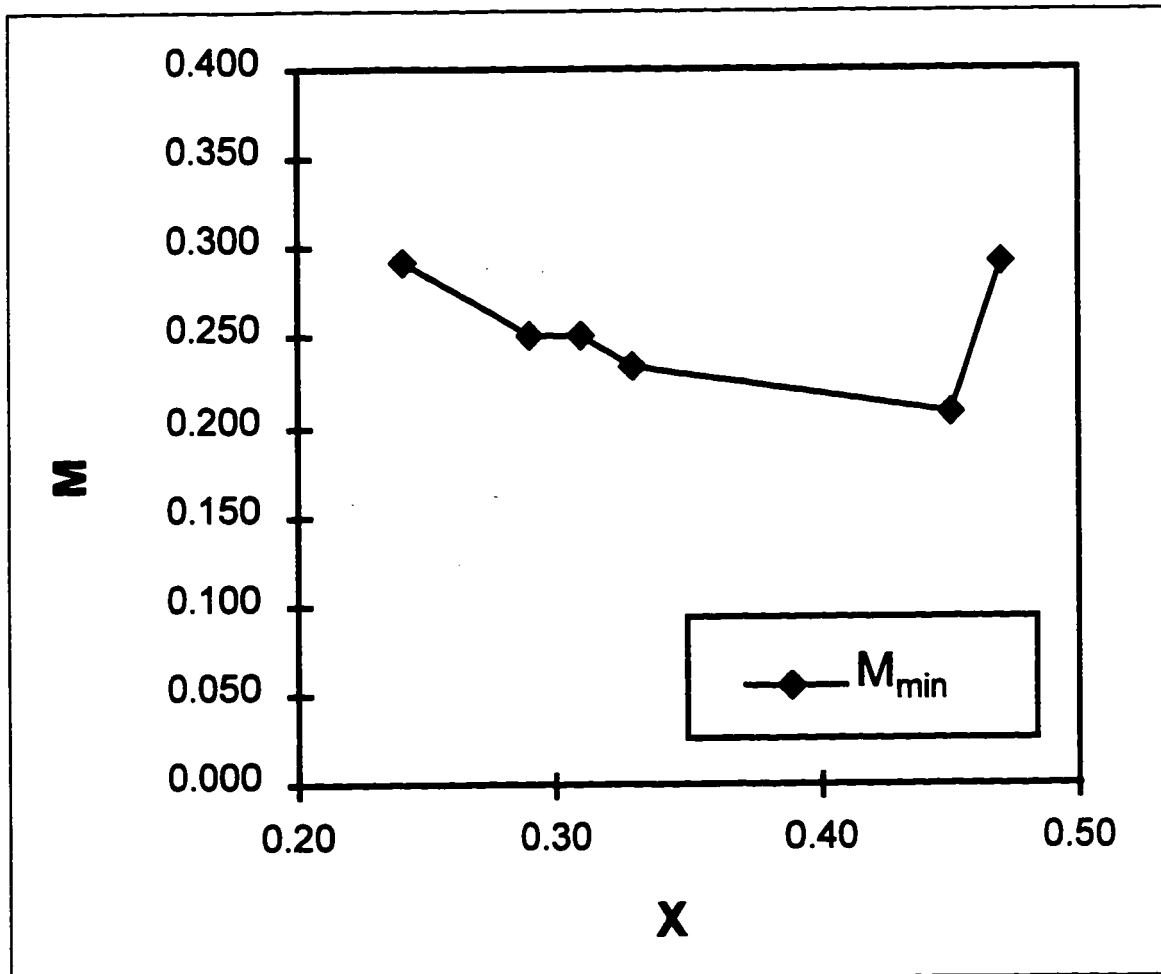


Figure 17: Vertical range fixed at 0.2 chords. $\alpha = 15^\circ$.

3.7.5 Reynolds Number and Sink Strength of Stable Vortices

A wide range of Re and M was observed for the stable vortices. Re ranged from 8400 to 55,000, while M varied from 0.293 to 0.878. Since the suction rate was kept constant for all tunnel velocities, the non-dimensional sink strength varied inversely to the Reynolds number as the tunnel velocity was increased and decreased. It is interesting to note that the non-dimensional sink

strengths were significantly below one. At $M = 1$, a given volume of the flow would be evacuated at the same rate that fluid entered the volume. It is highly desirable to have as little suction as possible, requiring less energy to maintain the vortex.

3.7.6 Lift and Drag

Measurement of the lift and drag forces on the plate was not possible in the smoke tunnel. Future work in a wind tunnel would allow measurement of these forces and possibly of the vortex strengths. This is an area that could be exploited by future work.

3.8 Conclusions

The following general observations were made:

1. Stable vortices were observed up to 40° angle of attack.
2. No vortices were observed for very small angles of attack (under 5°).
3. When the sink was placed very close to the surface of the plate (less than 0.1 chord lengths), re-attached flow was observed. It was also noted that the minimum vertical distance at which a stable vortex would form increased as the angle of attack was increased, leveling out at 0.13 chords above the plate for angles of attack between 15° and 25° .
4. As the sink was raised from the plate, the required suction maintaining the vortex grew.

5. Horizontal placement of the sink was surprisingly arbitrary, from 0.1 chords downstream of the leading edge to a full half chord downstream of the leading edge. However, a definite band of low sink strength vortices was found for each angle of attack.
6. The vortices with the lowest sink strengths lay as close to the plate as possible before re-attached flow occurred. The closer the vortex was to the plate; however, the smaller the range of dimensionless sink strengths became where the vortex was stable (Figure 11-Figure 14). Since sink strength was held constant while the freestream velocity of the tunnel was changed, a smaller range of dimensionless sink strengths implies a smaller range of acceptable velocities where a stable vortex would form.
7. At all angles of attack between 10° and 25° the lowest dimensionless sink strengths for stable vortex formation were found to be about 0.167. However, the upper limit on stable sink strengths increased with angle of attack. The larger the angle of attack, the larger the range of possible vortices. Since the sink strength was held constant, at low angles of attack vortex stability was very sensitive to the freestream velocity. For large angles of attack, sink locations were found which supported stable vortices even with large changes in velocity. These locations were farther above the plate than the lowest sink strength locations, but supported a greater range of velocities.

It can be concluded, based on these observations that stable vortices exist for a large range of angle of attack for the flat plate with suction. The vortices

formed with the weakest suction were found closer to the plate than the vortices formed with stronger suction. There also seems to be an implied trade off between the lowest sink strength required to maintain a vortex, versus the allowable variation in that sink strength (hence freestream velocity) while maintaining a vortex. Regardless of the angle of attack, sink strength could not be lowered beyond 0.135. Larger angles of attack permitted stronger sinks to be used before re-attached flow occurred.

These results are encouraging enough to suggest more rigorous testing of the model in a wind tunnel that would allow lift and drag forces to be measured. These recommendations and others are presented in section 5.

4. NUMERICAL ANALYSIS

4.1 Introduction

The incompressible Navier-Stokes equations were solved numerically for the flow over a 2% thick symmetrical airfoil (approximating a flat plate). The sink location and suction rate were set to produce steady state, detached vortices over the flat plate for a given angle of attack and Reynolds number. Sink location, suction strength, Reynolds number, and angle of attack all played an important role in producing stable vortices. Specific solutions, those matching the conditions presented in section 6 were obtained to compare with the smoke tunnel results.

4.2 Previous Work

A numerical analysis of Rossow's⁷ work utilizing both a fore and aft flap was performed by Todd Riddle using INS3D, a three dimensional version of INS2D. His analysis generated three-dimensional vortices that became trapped over the wing through the use of fences⁸. INS2D was chosen to perform my own numerical analysis of the flow.

4.3 The Code INS2D

INS2D was used to analyze the flow around the flat plate, both with and without the sink. This code was selected because it has already been used to model vortex/sink combinations³⁻⁵. INS2D is a fully viscous, incompressible, two-dimensional Navier-Stokes solver capable of running in either a steady state or

time accurate mode. The code employs artificial compressibility and uses a third order accurate flux-difference splitting for the convective terms and a second order accurate central difference for the viscous terms. The time accurate computations are obtained by sub-iterating the equations in pseudo-time for each physical time step. A line-relaxation scheme is used in both the time accurate and steady state computations that allows large pseudo-time steps in the time accurate solution and fast convergence rates in the steady state solution.

4.4 The Governing Equations

The Navier-Stokes equations for two-dimensional, incompressible flow (written in conservative form, and neglecting body forces):

Continuity

$$\frac{\partial u}{\partial x} + \frac{\partial v}{\partial y} = 0 \quad (4.1)$$

X Momentum

$$\rho \frac{\partial u}{\partial t} + \frac{\partial}{\partial x}(\rho u^2 + p - \tau_{xx}) + \frac{\partial}{\partial y}(\rho uv - \tau_{xy}) = 0 \quad (4.2)$$

Y Momentum

$$\rho \frac{\partial v}{\partial t} + \frac{\partial}{\partial x}(\rho uv - \tau_{yx}) + \frac{\partial}{\partial y}(\rho v^2 + p - \tau_{yy}) = 0 \quad (4.3)$$

Density can be eliminated from the momentum equations by substituting the following non-dimensional variables:

$$\tilde{u} = \frac{u}{U_\infty} \quad \tilde{v} = \frac{v}{U_\infty} \quad (4.4)$$

$$\tilde{x} = \frac{x}{L} \quad \tilde{y} = \frac{y}{L} \quad (4.5)$$

$$\tilde{\tau}_{xx} = \frac{\tau_{xx}}{\rho U_\infty^2} \quad \tilde{\tau}_{yy} = \frac{\tau_{yy}}{\rho U_\infty^2} \quad \tilde{\tau}_{xy} = \frac{\tau_{xy}}{\rho U_\infty^2} \quad \tilde{\tau}_{yx} = \frac{\tau_{yx}}{\rho U_\infty^2} \quad (4.6)$$

$$\tilde{t} = \frac{t U_\infty}{L} \quad \tilde{p} = \frac{p}{\rho U_\infty^2} \quad (4.7)$$

Giving :

$$\frac{\rho U_\infty^2}{L} \left[\frac{\partial \tilde{u}}{\partial \tilde{t}} + \frac{\partial}{\partial \tilde{x}} (\tilde{u}^2 + \tilde{p} - \tilde{\tau}_{xx}) + \frac{\partial}{\partial \tilde{y}} (\tilde{u}\tilde{v} - \tilde{\tau}_{xy}) \right] = 0 \quad (\text{X Momentum}) \quad (4.8)$$

$$\frac{\rho U_\infty^2}{L} \left[\frac{\partial \tilde{v}}{\partial \tilde{t}} + \frac{\partial}{\partial \tilde{x}} (\tilde{u}\tilde{v} - \tilde{\tau}_{xy}) + \frac{\partial}{\partial \tilde{y}} (\tilde{v}^2 + \tilde{p} - \tilde{\tau}_{yy}) \right] = 0 \quad (\text{Y Momentum}) \quad (4.9)$$

These equations can then be written as a single equation by using the following vector substitutions:

$$\vec{u} = \begin{bmatrix} \tilde{u} \\ \tilde{v} \end{bmatrix} \quad e = \begin{bmatrix} \tilde{u}^2 + \rho \\ \tilde{u}\tilde{v} \end{bmatrix} \quad f = \begin{bmatrix} \tilde{u}\tilde{v} \\ \tilde{v}^2 + \rho \end{bmatrix} \quad e_v = \begin{bmatrix} \tilde{\tau}_{xx} \\ \tilde{\tau}_{xy} \end{bmatrix} \quad f_v = \begin{bmatrix} \tilde{\tau}_{xy} \\ \tilde{\tau}_{yy} \end{bmatrix} \quad \dots \quad (4.10)$$

Where the subscript v, denotes the viscous flux terms.

This allows us to write both momentum equations as one vector equation, without density:

$$\frac{\partial \vec{u}}{\partial \tilde{t}} + \frac{\partial}{\partial \tilde{x}} (e - e_v) + \frac{\partial}{\partial \tilde{y}} (f - f_v) = 0 \quad (4.11)$$

4.5 The Mesh

To perform the numerical analysis described above, a grid must be constructed to meet the following conditions. Firstly, a numerical domain has to be constructed to approximate the physical flow boundaries of the problem. Numerical boundary conditions must be stated at these points. Secondly, a grid

must be constructed to provide enough computational nodes in all flow regions to obtain an accurate solution.

As described earlier in section 3.3, the physical domain that we wish to model is that of a 3 ft x 3 ft x 2.5 in smoke tunnel. Since the smoke lines are observed to remain in two dimensions (with the exception of the vortex core itself), we can approximate the wind tunnel experiment by using a two dimensional analysis. To further simplify the mesh generation, it was assumed that the wind tunnel top and bottom walls were sufficiently far away from the test model so that they did not have to be included as closed boundary conditions to the INS2D solver.

A C-mesh was generated around the airfoil using the hyperbolic grid generator, HYPGEN⁹. The C-mesh contained 241 circumferential nodes and 61 radial nodes. 161 of the circumferential nodes surrounded the airfoil, and 41 nodes were used to model the wake (see Figure 18 and Figure 19). The cell size in the area of interest, that of the vortex location, was approximately 0.02 by 0.02 chords.

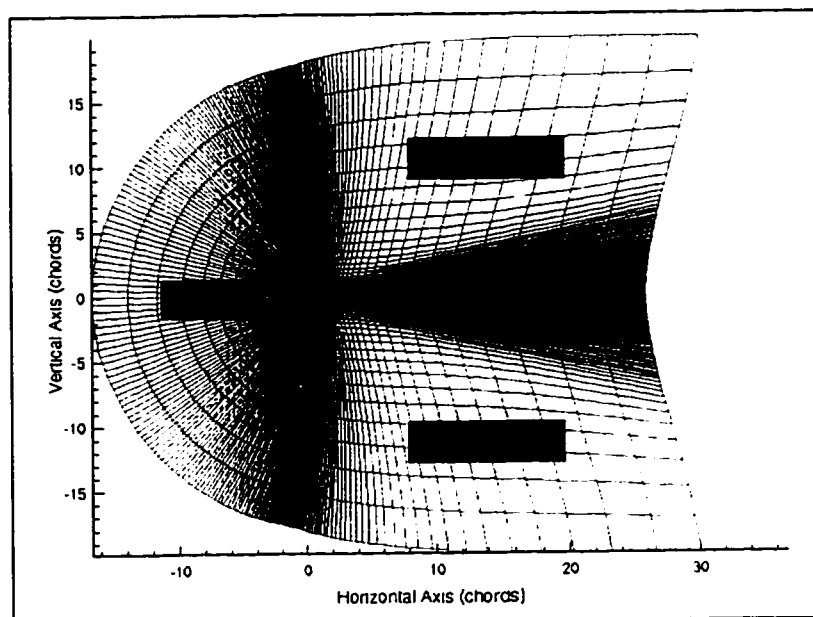


Figure 18: The complete mesh used by INS2D.

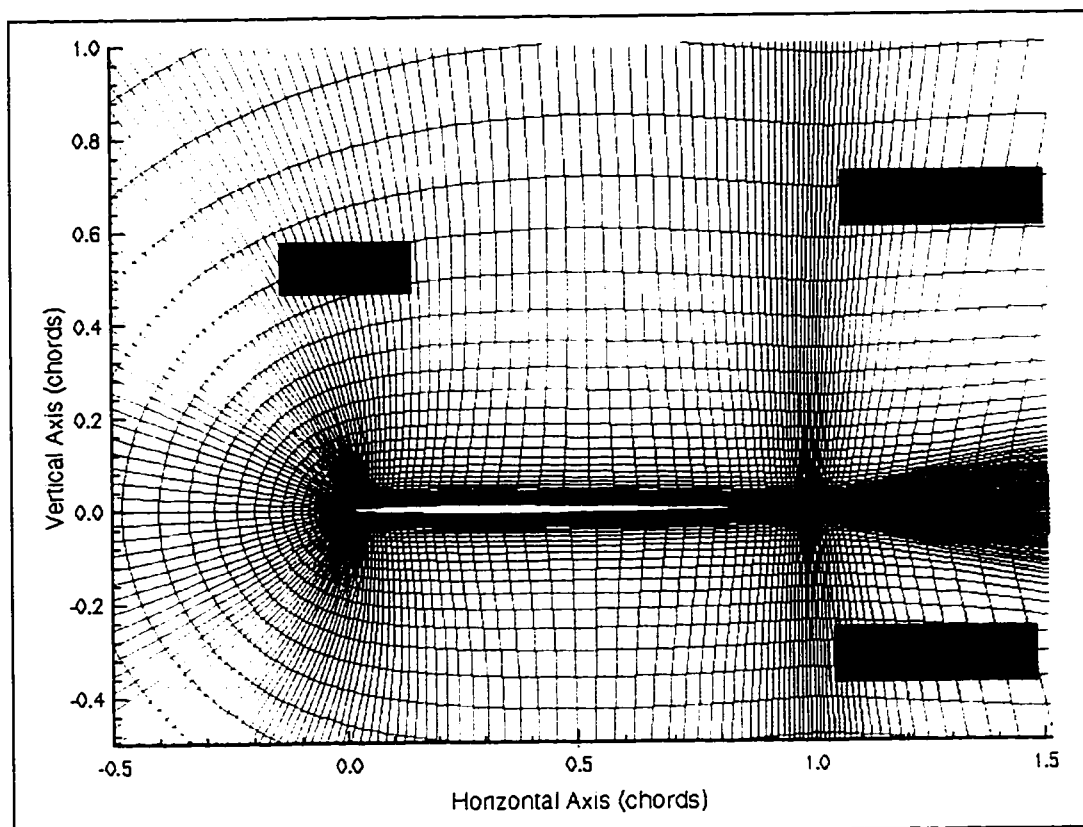


Figure 19: A close-up of the mesh surrounding the NACA 0012 airfoil.

4.6 Boundary Conditions

4.6.1 Boundary Conditions Supplied to INS2D

The INS2D boundary conditions were stored in a file called BCMAIN.DAT.

An example of this file is shown here.

Table 2: INS2D's Boundary Conditions Input File (BCMAIN.DAT)

c Flow over airfoil:						
c-----						
c	ibcval	zone	jbeg	jend	kbeg	kend
c-----						
c						
	31	1	1	1	1	-1
	31	1	-1	-1	1	-1
c						
	0	1	41	201	1	1
	25	1	2	-2	-1	-1
	60	1	2	40	1	1
	60	1	202	-2	1	1
c						
c These determine the position of the sink						
c						
	4	1	172	172	33	34
	5	1	171	171	33	34

This file was only edited when the location of the sink was changed. The *ibcval* variable identifies the particular boundary condition assigned to the listed grid points. The parameter *zone* defines the flow field zone (in this case there is only one flow zone). The parameters *jbeg*, and *jend* specify the circumferential nodes that a particular *ibcval* applies to. Likewise, *kbeg* and *kend* specify the radial nodes that a particular *ibcval* applies to. Descriptions of the values used for *ibcval* in the computational runs are compiled in table 3.

Table 3: INS2D Boundary Conditions

<i>ibcval</i>	Boundary Condition
0	No slip, wall normal vector pointing in the positive computational direction
4	Moving no-slip wall, with wall normal vector pointing in the positive computational direction
5	Moving no-slip wall, with wall normal vector pointing in the negative computational direction.
25	C-grid outer boundary, velocity field determined by a vortex at the $\frac{1}{4}$ chord point
31	Outflow boundary using extrapolated velocities and constant static pressure.
60	C-grid wake cut boundary. These points will be updated by averaging values from surrounding points. Normal surface vector points in the negative computational direction.

4.6.2 The Plate

The flat plate was modeled as a 2% thick symmetric airfoil (NACA 0012). This airfoil has a maximum thickness at the quarter-chord location, and is a reasonable approximation to the flat plate used in the smoke tunnel experiment. The plate used in the smoke tunnel was uniformly 1.6% thick. The parameter *ibcval* was set to 0 for nodes on the surface of the airfoil.

4.6.3 The Freestream

A bound vortex was used at the $\frac{1}{4}$ chord point of the airfoil to generate an approximate velocity field. This was added to a uniform velocity field at the given angle of attack. The resulting ideal, inviscid flow field solution was used to

initialize the mesh values at the start of the computation. The bound vortex mentioned above should not be mistaken for the singularity introduced artificially in this experiment. The sole purpose of this vortex is to generate an approximate velocity field to initialize the mesh values at the start of the computation. The parameter *ibcval* was set to 25 for nodes laying on the airfoil. Boundary grid points at the exterior edge of the C-mesh were treated as extrapolated velocities at constant static pressure; the parameter *ibcval* was set to 31 for these boundary points.

4.6.4 The Sink

Taking a single computational cell made up of four grid points, and setting the four grid points as interior velocity boundary conditions, an artificial sink was created. A velocity was given at each of these four points to generate the required mass removal rate. This velocity is referred to as V_{sink} and is fixed across the boundary of the computational cell divided by the freestream velocity. V_{sink} can be related to the non-dimensional sink strength through the following relation:

$$V_{sink} = \frac{Ms}{L} \quad (4.12)$$

Where s is the span of the wind tunnel in meters and L is the perimeter of the computational cell used for the sink in chords.

4.6.5 The Wake

The boundary points of the wake cut were treated as image points. The parameter *ibcval* for these points was set to 60.

4.6.6 Turbulence Modeling

Despite the low Reynolds number, no laminar solutions were found. Sharp separation occurs at the leading edge that requires the stabilizing influence of a turbulence model to achieve convergence. INS2D is capable of both laminar and turbulent calculations. For turbulent calculations, the solver uses a Reynolds time-averaged form of the basic equations. Using the Boussinesq approximation, the viscous flux terms in the time-averaged equations are expanded.

$$\tau_{ij_{total}} = \tau_{ij_{lam}} - \overline{\rho u_i' u_j'} = (\nu + \nu_t) \left(\frac{\partial \tilde{u}_i}{\partial x_j} + \frac{\partial \tilde{u}_j}{\partial x_i} \right) \quad (4.13)$$

The eddy viscosity term in the above equation was solved by INS2D using the Baldwin-Barth turbulence model¹⁰. This turbulence model was used because it does not employ an algebraic length scale, allowing for easy computation even in problems with multiple shear or boundary layers (such as the current problem). Algebraic models are faster but do not apply in this case. Also, this one-equation turbulence model is very fast, and CPU time was a factor in considering different models.

4.7 Procedure

Each computational run of INS2D requires modifications to two separate input files, BCMAIN.DAT and AF.IN. BCMAIN.DAT has already been described in section 4.6.1. For each run, the location of the sink was determined by the values *jbeg*, *jend*, *kbeg* and *kend* specified in BCMAIN.DAT for the sink. The AF.IN file contains all of the other information necessary to run INS2D. The values in AF.IN that changed between runs were *reynum* (the Reynolds number), *alpha* (the angle of attack) and *vsink* (the non-dimensional sink strength). An example of the AF.IN file and an explanation of all of its variables can be found in Appendix B.

A solution was considered to be converged if the measure of the divergence of the velocity field (*resmax*) fell below $1e^{-5}$ within 200 iterations. Converged solutions were stored, downloaded, and viewed using Tecplot¹¹ to produce the images used in this document.

4.8 Results

4.8.1 Locating a Stable Vortex

Using the experimental results as a starting point, a vortex was first placed at $(X, Y) = (0.30, 0.17)$, while the airfoil was placed at 15° angle of attack, corresponding to a large grouping of stable vortices found in the smoke tunnel experiment. At this location in the experiment, stable vortices were produced between Re of 8,430 and 29,504 (corresponding to non-dimensional sink

strengths of 0.251 and 0.878). A Re of 25,200 was chosen to run the computational trial with a corresponding sink strength of 0.251. A value of 25,200 was chosen because it represented a middle velocity (of 3.5 m/s) at wind tunnel conditions, with an M of 0.251, the corresponding experimental sink strength. Convergence with M set to 0.251 (the lower bound of the experimental sink strength) was not obtained at this Reynolds Number. By varying the sink strength between the minimum and maximum sink strengths associated with the experimental vortex, a converged solution was found at $M = 0.878$, the upper range of sink strengths observed in the experiment (but at a Re of 25,200).

Solutions that did not converge appeared to be unsteady flows. A time-accurate solution was not attempted for these flows. However, viewing the flow at different iterations showed the vortex form and shed in an oscillatory fashion. The lift coefficient could be observed to cycle from a high value to a low value as the vortex formed and detached. The flow observed was similar to the flow shown in Figure 33 (the flow around the airfoil without a sink).

Once a converged solution had been found, another computational run at $M = 0.878$ was made with the demonstrated experimental Re value of 8,430. A converged solution was found at these values, duplicating experimental values. The resulting flow pattern was plotted against an image taken directly from the wind tunnel tests. In the computational plot, the streamlines were added to simulate the actual smoke lines used in the experiment. Except for the separation of the flow caused by the sting of the experimental model, the two flow

patterns are nearly identical. The scale of each image is as close to identical as possible. Each experimental streamline can be matched to its computational counterpart. The formation of the vortex seemed to be much more sensitive to M than to Re .

INS2D vortex solutions did not exactly duplicate the range of Re and M found in the experiment. However, at least some of the observed experimental flows had similar computational solutions in INS2D. Unfortunately, while the solution at $(X,Y) = (0.30, 0.17)$, $Re = 8,340$, $M = 0.878$, $\alpha = 15^\circ$, matched a flow observed in the smoke tunnel, there was not enough flexibility in this solution to provide data for a meaningful computational analysis. An INS2D solution found at $(X,Y) = (0.30, 0.17)$, $Re = 25,200$, $M = 0.664$, generated many more converged solutions when its parameters were varied. This solution was used as a base for the remaining computational analysis.

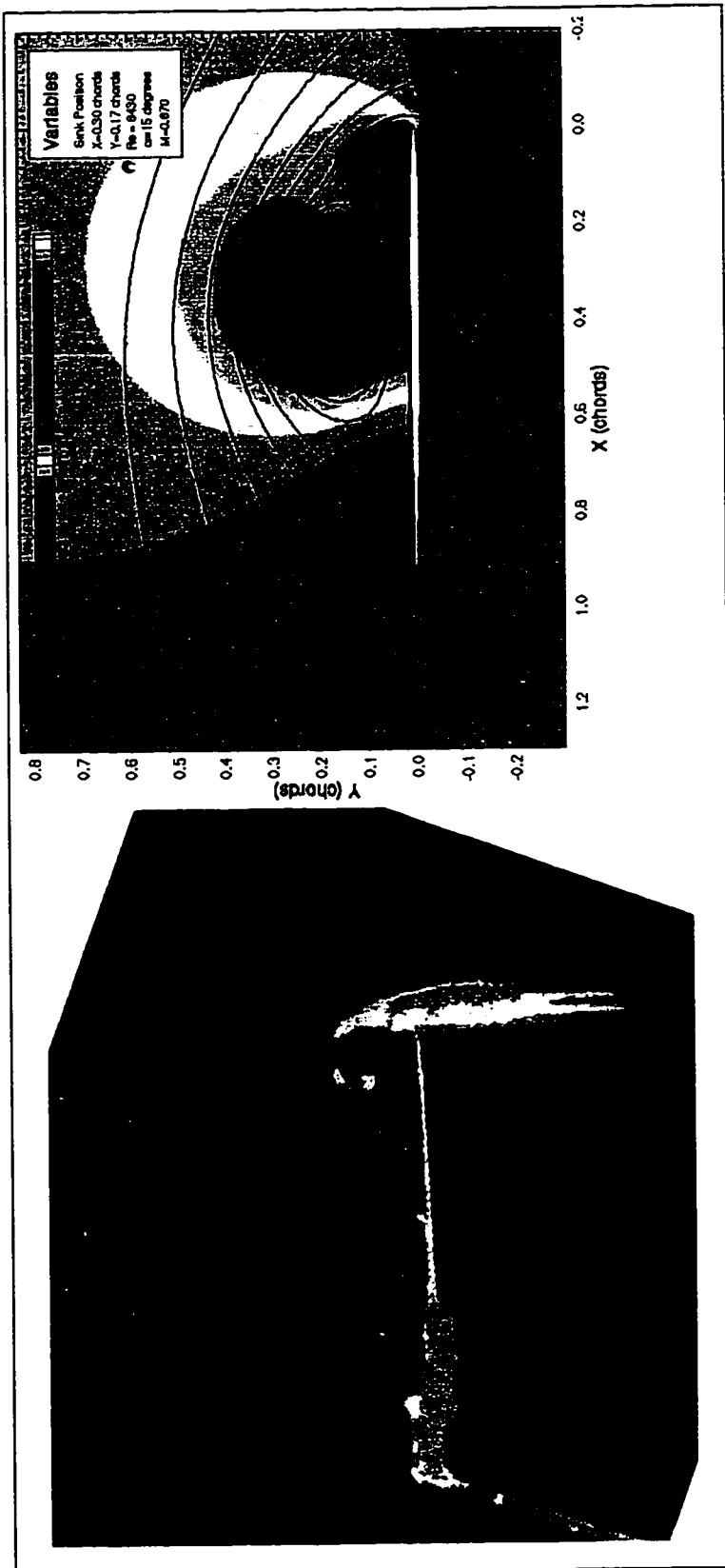


Figure 20: Experimental vortex and computational vortices at $\alpha = 15^\circ$.

$M = 0.878$, $Re = 8430$, $V = 1.0$ m/s for each case. $c_l = 3.04$, $c_d = 0.653$, and $c_m = -0.108$ in the computational case. The experimental image has been rotated to provide a better contrast between the flows.

4.8.2 Reynolds Number Effects

Using the experimental results as a launching point, the most seemingly stable vortex location of $(X, Y) = (0.30, 0.17)$, $M = 0.664$ at 15° angle of attack), was chosen to investigate the existence of vortex solutions based on Reynolds number. Several INS2D trials were run, varying Re between 1 and 1,000,000 (table 4).

Table 4: Reynolds Number Dependence of Vortex Formation

Re	Result	Stagnation Points (lower/upper)	
1	Did not converge	N/A	N/A
10	Converged	0.0	0.70
100	Converged	0.04	0.82
11,000	Converged	0.07	0.62
25,200	Converged	0.07	0.63
100,000	Stable solution but did not meet convergence criteria	0.07	0.64
1,000,000	Did not converge	N/A	N/A

The results showed the existence of vortices in the range of Re between 10 and 25,200. Figures comparing the flow field solutions at $Re = 100$, 11,000, and 100,000 are shown below. The flows at $Re = 100,000$ appeared stable, but never reached the convergence criteria of $res_{max} < 10^{-5}$. Convergence at $Re = 100,000$ probably could have been reached with enough computational cycles. Outside of those ranges, no converged solutions were found.

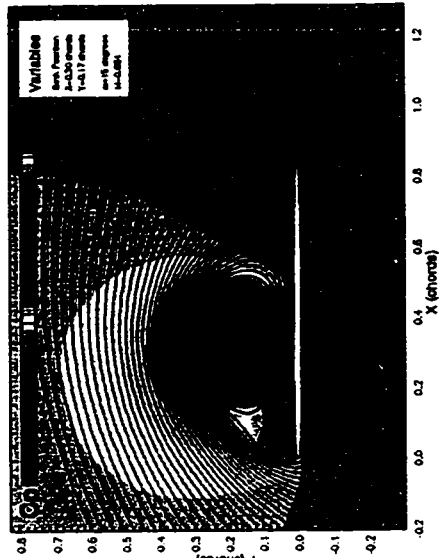
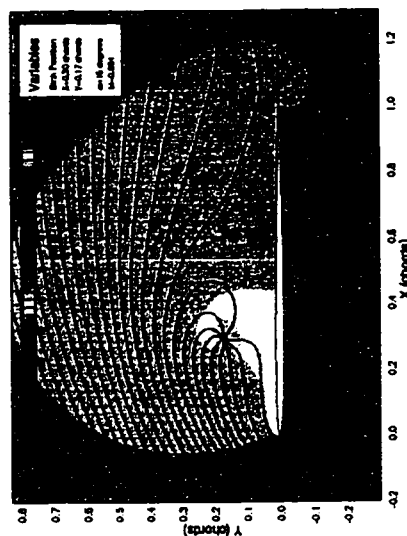
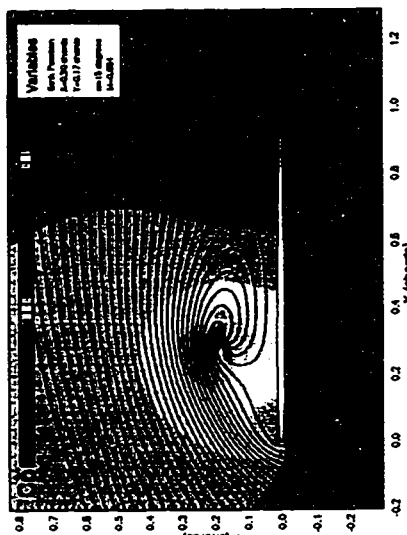
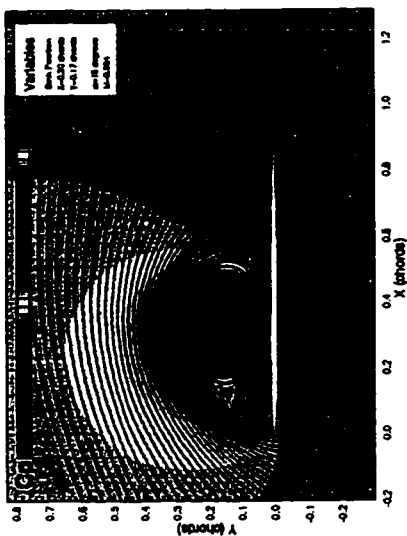
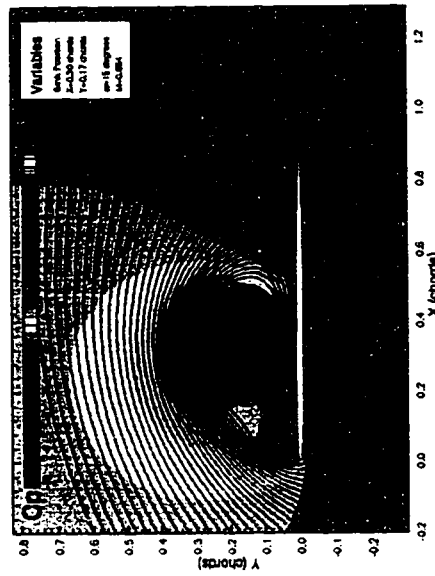
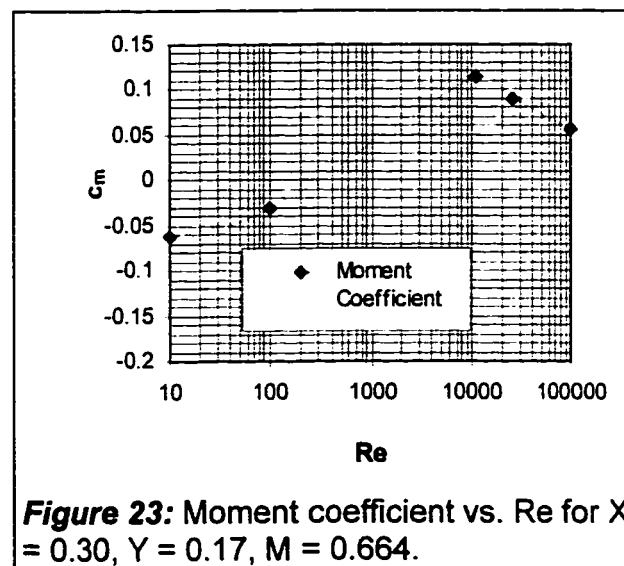
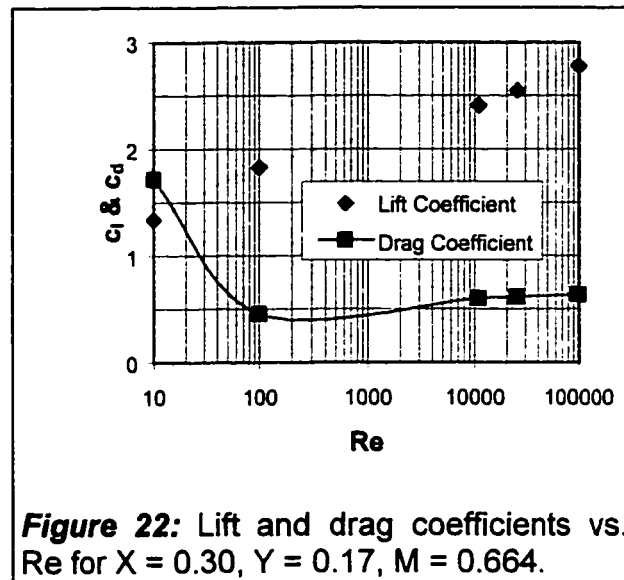


Figure 21: Vortex flow patterns computed at different Reynolds numbers.
 From top left, to bottom right:
 Re = 10, 100, 11,000, 25,200, 100,000.



Lift, drag and moment coefficients for the various Reynolds numbers are given in Figure 23 and Figure 22 below.



Two flow characteristics become immediately apparent while observing the flow patterns in Figure 21 - the size of the vortex and the pressure coefficient

at the core of the vortex. At both high and low Re the flow around the vortex seems to reattach to the plate at about 0.65 chords downstream of the leading edge. The pressure coefficient at the core of the vortex also decreases as Re increases, explaining both the increased lift and increased moment coefficient at higher Re numbers. Lift and drag increase steadily as Re number increases.

4.8.3 Vortex Dependence on Angle of Attack

To test the vortex formation at various angles of attack, the vortex location at $(X, Y) = (0.30, 0.17)$ was again chosen. Runs were made with constant sink strengths of 0.664. Converged solutions were found for angles of attack between 5 and 20 degrees. Outside of those angles, no converged solutions were found. By studying the five flow patterns in Figure 24-Figure 27, we can observe how angle of attack changes the flow around the plate. At larger angles of attack, both the upper and lower stagnation streamlines move farther downstream on the plate. Both lift and drag increase significantly at larger α (Figure 29 and Figure 28).

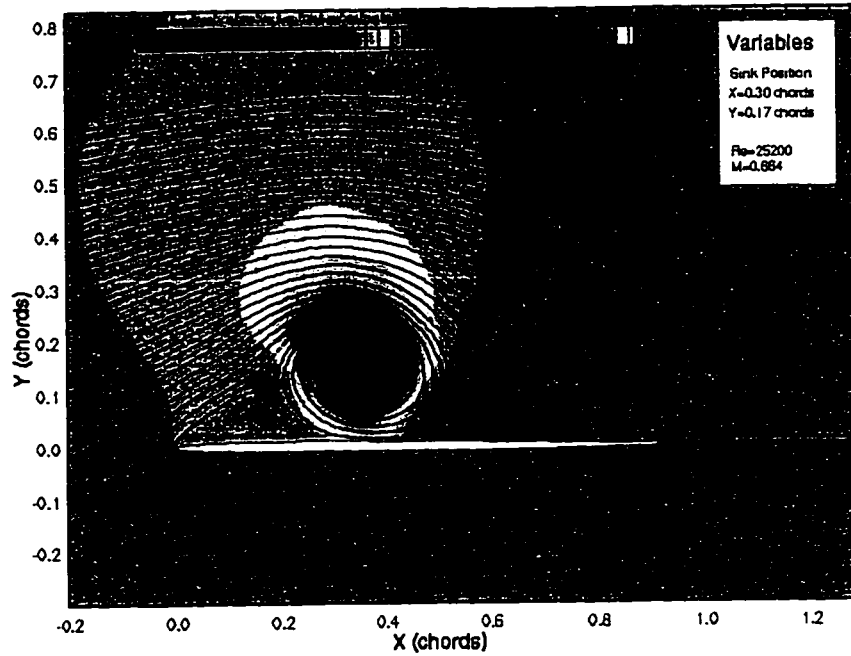


Figure 24: Vortex flow at 5° angle of attack

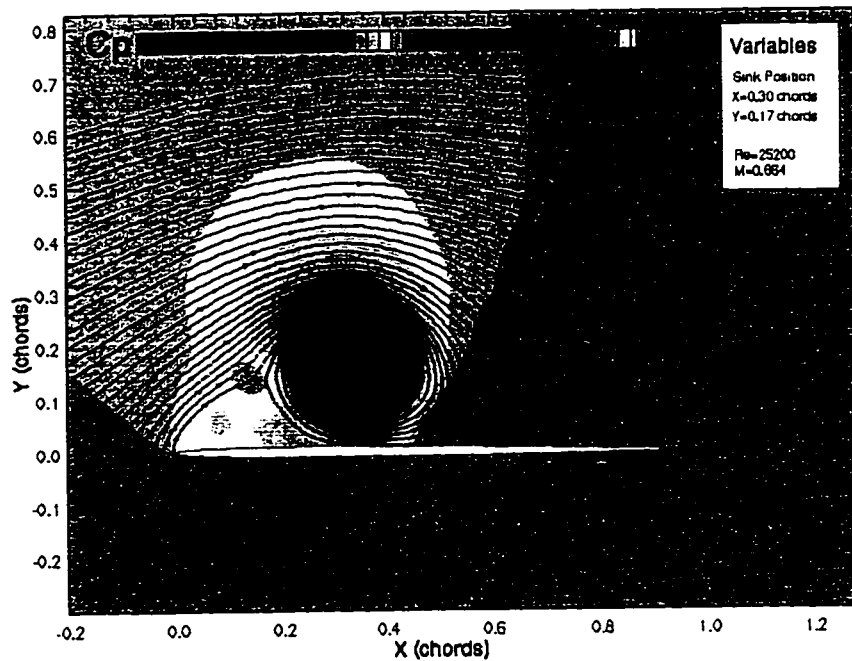


Figure 25: Vortex flow at 10° angle of attack

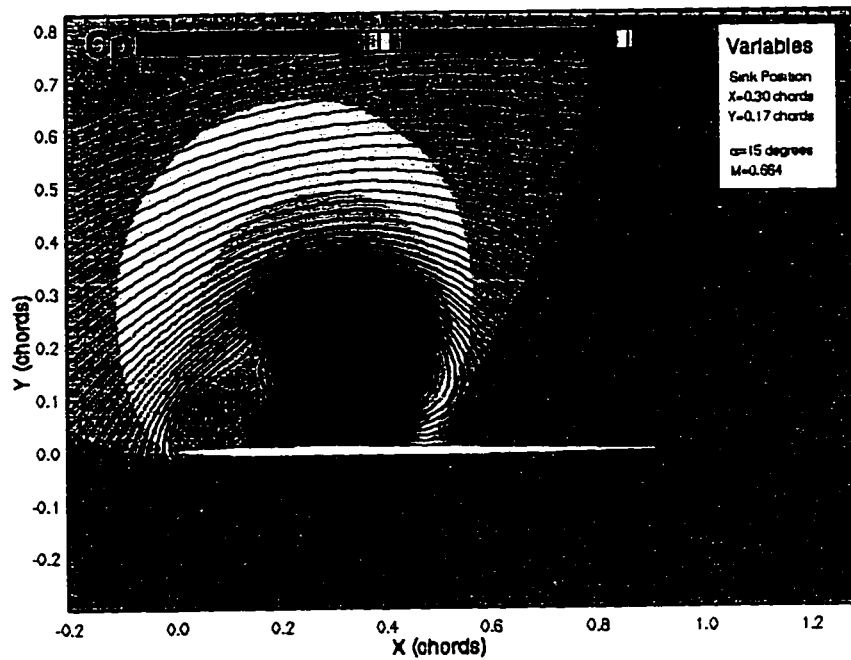


Figure 26: Vortex flow at 15° angle of attack

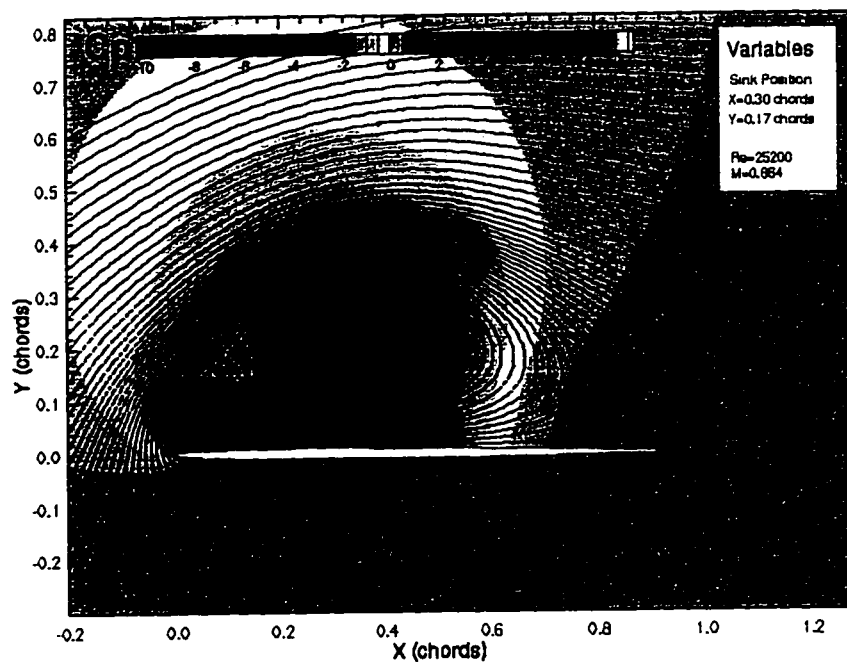
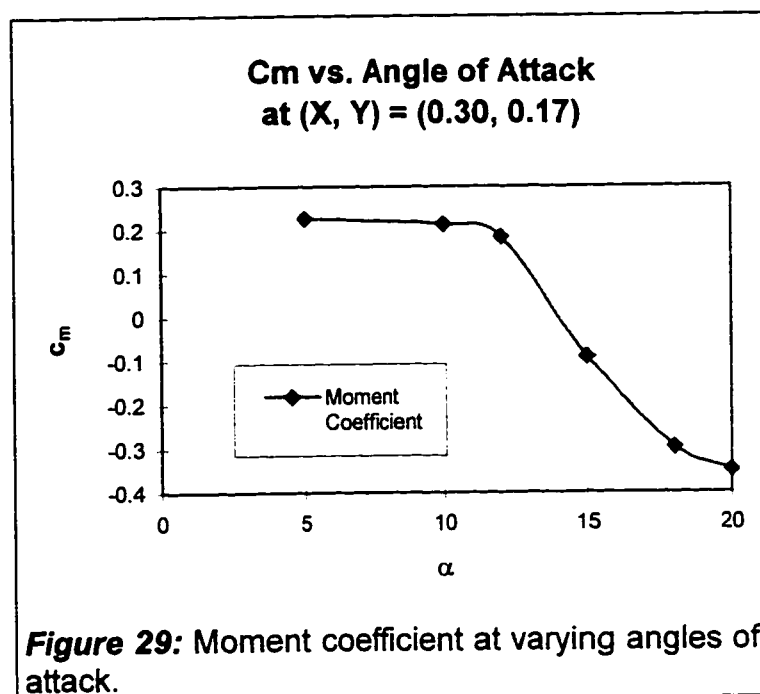
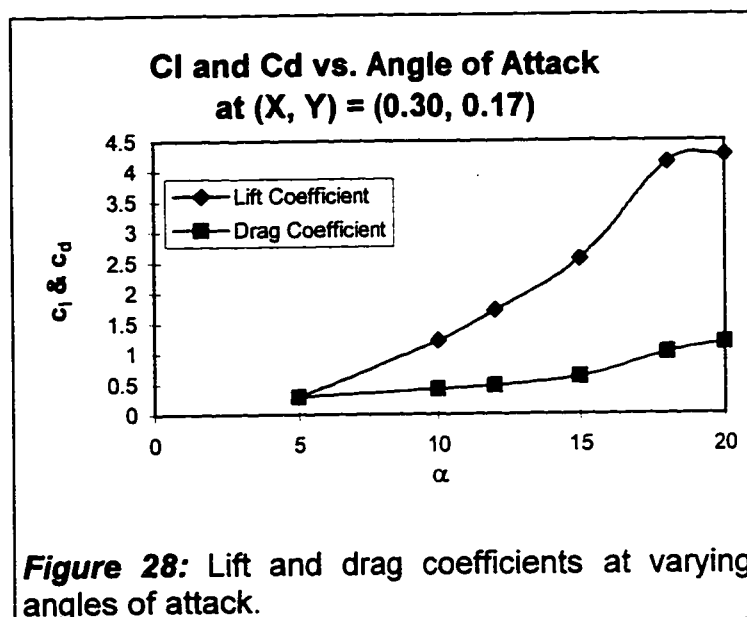


Figure 27: Vortex flow at 20° angle of attack



One problem that exists with the computational model is that the sink position and strength must be placed into the computation artificially, instead of running the computation and capturing the sink location and strength (much like shock fitting and capturing methods). While it would be valuable to observe the change in sink strength and location as angle of attack was varied, we cannot capture this transition with the current method. What can be done is to determine at what point modifying the angle of attack prevents a converged solution from being reached thus settling on a range of alpha that will permit a certain vortex to exist. A hypothesis can then be tested, such as: will the vortex move outwards from the plate as angle of attack is increased? To do this, an additional test with the vortex placed one computational cell further away from the plate at the highest angle of attack previously determined to produce a converged solution. If the solution converges, then another trial can be made, increasing only the angle of attack. If the hypothesis is correct, perhaps solutions at even higher angles of attack will converge.

The above hypothesis was tested using a vortex location of $(X, Y) = (0.30, 0.20)$, with M continuing to be held constant at 0.664. Some converged solutions were found at this location; however, angles of attack greater than 20° did not produce any converged solutions, even over a large range of Re from 11,000 to 1,000,000. A similar test was performed at a vortex location of $(X, Y) = (0.30, 0.14)$ for lower angles of attack. This time no converged solutions were found at any Re or α . Due to the large numbers of trials that would have to be

run, this relationship was not explored further at other vortex locations, sink strengths, and/or Re.

4.8.4 Vortex Flows at Varying Downstream Stations

In the previous section, an attempt was made to find vortices at vertical locations other than $Y = 0.17$. Vortices were only found at the next highest vertical station ($Y = 0.20$), and those were limited in number, occurring only at smaller ranges of α and Re than their counterparts at $(X, Y) = (0.30, 0.17)$. It was deemed that not enough data could be generated in the vertical plane to produce any significant correlation. The horizontal dimension proved to yield much more information.

In the horizontal plane above the plate, vortices were found for $0.23 \leq X \leq 0.37$ at $Y = 0.19$. The lift, drag and moment coefficients of these vortices are shown in Figure 30 and Figure 31. Vortices were found farther down the plate,

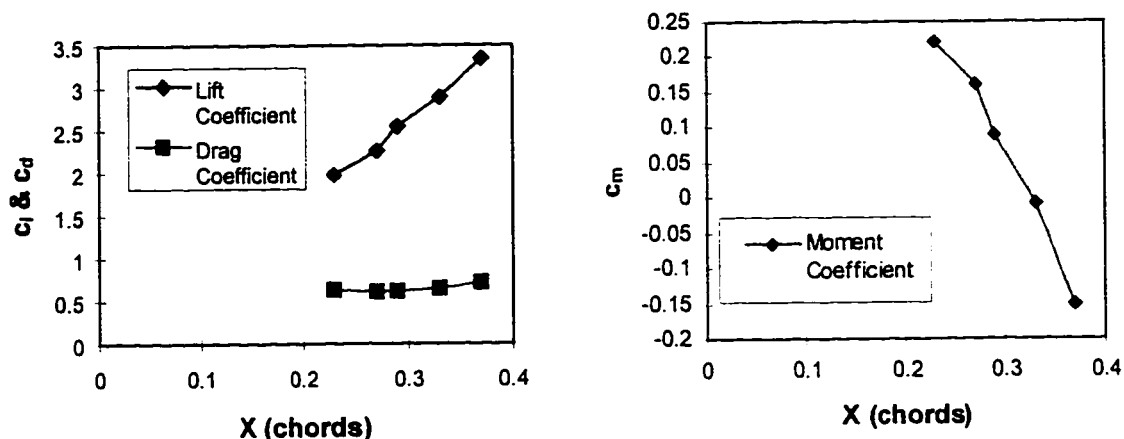


Figure 30: Lift and drag coefficients at various distances from the LE.

Figure 31: Moment coefficient at various distances from the LE.

as far as 0.46 chords downstream of the LE (and as close as $X = 0.20$ chords), but at a larger distance from the airfoil ($Y = 0.20$). Four plots showing the flow at the vertical station of $Y = 0.17$ are shown in Figure 32.

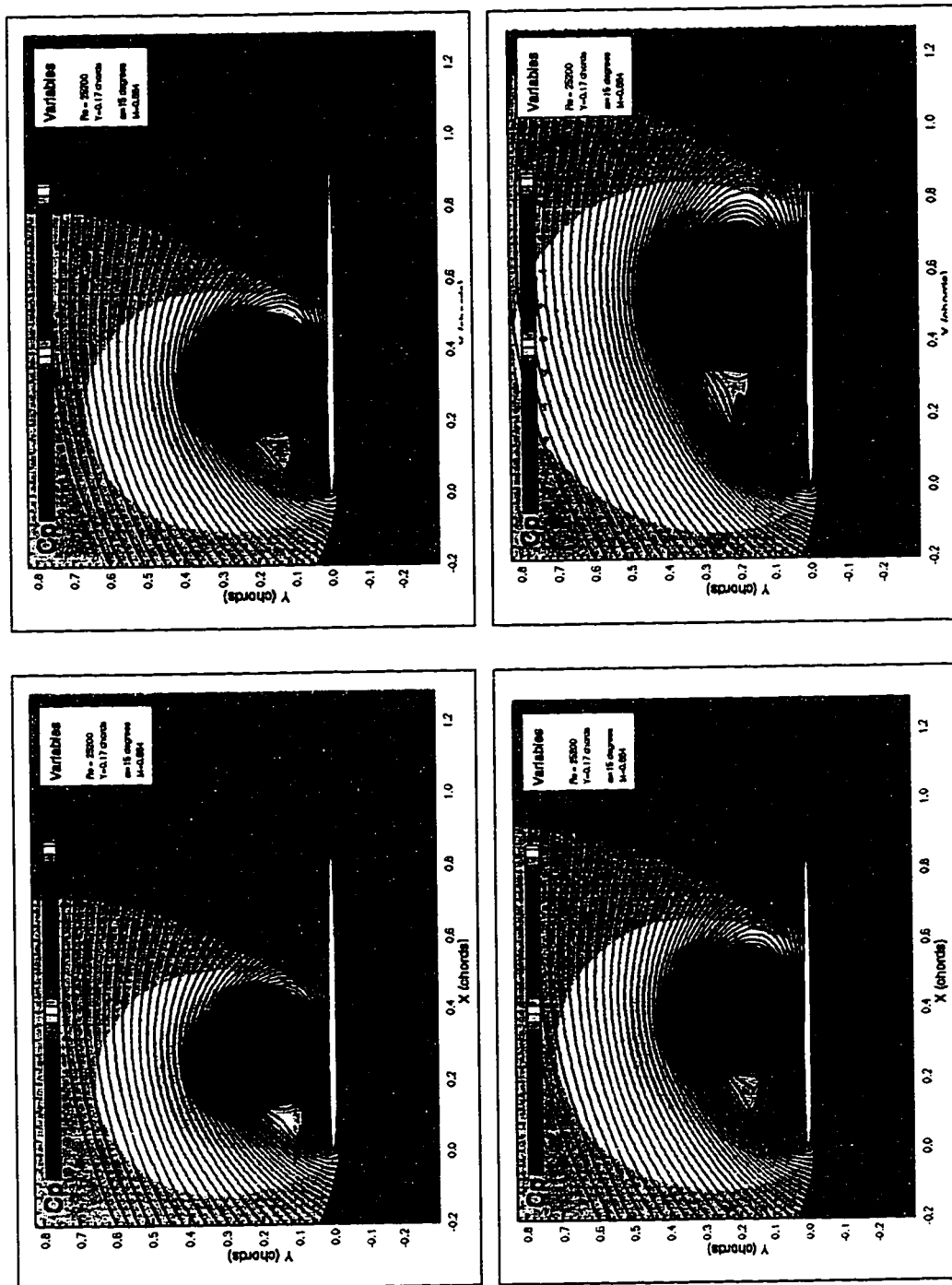


Figure 32: Vortex flow at four separate horizontal distances from the LE of the airfoil. From top left to bottom right: $X = 0.23, 0.30, 0.37, 0.45$. At $X = 0.45$, the counter-rotating LE vortices are shown.

4.8.5 Discrepancies

There are many possible reasons for discrepancies between the computational results and the experimental data. The smoke lines made two complete revolutions before becoming indistinct at the core of the vortex (about the size of the suction orifice). This indicates that we have two-dimensional flow until we reach the core of the vortex (where the fluid starts traveling towards the orifices in the spanwise direction). While it is not known precisely what this effect has on the two dimensional assumption of the computational solution, computational solutions did compare favorably with the experimental results. The non-dimensional area of the sink was $0.0069 \text{ m}^2/\text{m}^2$, while the cell size averaged about $0.0015 \text{ m}^2/\text{m}^2$ for the computational sink. Thus the computational sink is smaller than the "core" of the vortex.

The INS2D solutions all contained two counter-rotating vortices at the leading edge of the plate. These vortices were not observed in the smoke tunnel testing; however, smokelines may not have been in position to show these vortices and observation would have been difficult.

There was also significant error margins present in all of the experimental measurements that could lead to discrepancies. These error margins are listed in Table 1. The major error is the up to 24% uncertainty in the experimental Reynolds number.

The experimental flat plate was modeled as a 2% thick symmetrical airfoil. Although having approximately equal maximum thickness, the rounded leading edge and tapered trailing edge of the NACA 0012 airfoil modeled in INS2D could contribute to errors.

4.8.6 Flow Without the Sink

Above two degrees angle of attack, no steady flow solution was found for the flat plate. Without the sink, the flow is fully separated. Time-accurate computations had to be used for the separated flow case (indeed, no steady state solution exists for this flow). The addition of the sink in the proper location with the proper non-dimensional sink strength allows us to obtain the steady-state solution observed in the smoke tunnel. A time-accurate computation at 15° angle of attack and a Re of 25,200 shows separated flow and vortex shedding (Figure 33). Each frame is 0.1 seconds.

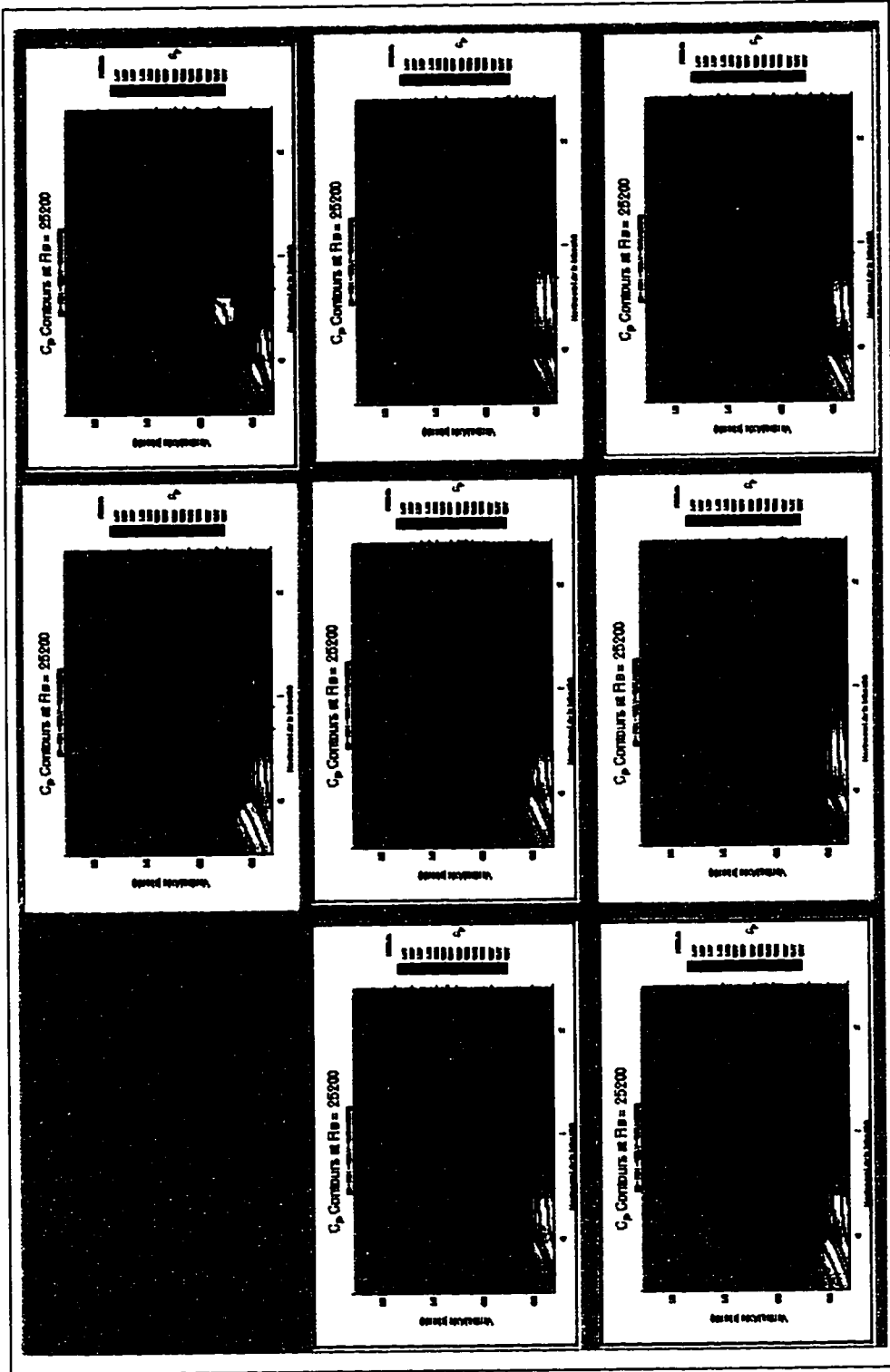


Figure 33: Unsteady flow at $\alpha = 15^\circ$, $M = 0.664$, $Re = 25\,200$, $(X, Y) = (0.30, 0.17)$.

4.9 Conclusions

There exist for some of the experimentally demonstrated vortices comparable solutions generated by INS2D. The flow patterns generated by both methods suggested that a two dimensional approach to solving the flow problem was valid. In one demonstrated case, identical flow conditions generated a nearly identical flow pattern.

It is not possible to say which experimental vortices could not be simulated by INS2D, since the allowable sink strength range for vortex formation in the experiment seemed to be much greater than that allowed by INS2D. So even though in some cases a trial or two did not produce a vortex flow, there could be other sink strengths that would allow a vortex to form. The computational analysis showed that the converged solutions were much more sensitive to sink strength than to Re , α , or sink location.

Solutions with a vortex did lead to increased lift coefficients at reasonable drag and suction values and were stable over a large range of Re . The only barriers that were observed for using these vortices in real life applications would be the low Re of the solutions observed and the efficient removal of the fluid over the wing. No solutions were observed for Re greater than 10^5 , considerably below the values required for either commercial or military aircraft.

It was not possible to test the entire range of vortices found experimentally. Since a "sink fitting" technique had to be employed, there was a

lot of trial and error involved in locating converged solutions. The conditions that generated the vortex in figure 22 were not found until more than 100 computational runs had been made. A "sink capturing" method would certainly aid the analysis of the experimental vortices.

5. SUMMARY AND RECOMMENDATIONS

5.1 Smoke Flow Visualization

The most frustrating limitation of the smoke tunnel experiment was the inability to measure lift and drag. Having found similar experimental and computational vortices, it would be of great interest to compare their lift and drag coefficients. Further experiments in a larger wind tunnel would also allow higher Reynolds number flows to be explored. Increasing the span and Reynolds number of the wind tunnel could create additional problems, however; increased suction would be required and increased three-dimensional flow patterns would result. Laser doppler velocimetry or other methods could be used to obtain velocity measurements in the vortex, enabling the strength of the vortex to be calculated.

No study was made of the reattached flow pattern that was observed during the smoke tunnel experiment. A further study of this three-dimensional flow pattern could be interesting.

5.2 Numerical Analysis

A NACA 0012 airfoil was modeled in INS2D using a C mesh. This was used to approximate the flat plate used in the smoke tunnel experiment. A more accurate computation could be achieved by modeling the flat plate in INS2D using a flat plate in an H mesh.

INS2D appeared to be adequate for analyzing the smoke tunnel flow. A three dimensional analysis could be attempted, but because of the exponential increase in computational time required, such an analysis may not be judicious.

REFERENCES

1. Saffman, P.G. and Sheffield, J.S. Flow over a Wing with an Attached Free Vortex. *Studies in Applied Mathematics*, No. 57, 1977, pp. 107-117.
2. Mourtos, Nikos J. and Brooks, Marcus. Flow past a Flat Plate with a Vortex/Sink Combination. *Journal of Applied Mechanics*, No. 63, June 1996, pp. 543-550.
3. Rogers, Stuart E. and Kwak, Dochan. An Upwind Differencing Scheme for the Time-Accurate Incompressible Navier-Stokes Equations. *AIAA Journal*, Vol. 28, No. 2, February 1990, pp. 253-262.
4. Rogers, Stuart E. and Kwak, Dochan. An Upwind Differencing Scheme for the Incompressible Navier-Stokes Equations. *Applied Numerical Mathematics*, Vol. 8, 1991, pp. 43-64.
5. Rogers, Stuart E. and Kwak, Dochan. Steady and Unsteady Solutions of the Incompressible Navier-Stokes Equations. *AIAA Journal*. Vol. 29, No. 4, April 1991, pp. 603-610.
6. Huang, M. and Chow, C. Trapping of a Free Vortex by Joukowski Airfoils. *AIAA Journal*, Vol. 20, No. 3, March 1982, pp. 292-298.
7. Rossow, V. J. Lift Enhancement by an Externally Trapped Vortex. *Journal of Aircraft*, Vol. 15, No. 9, September 1978, pp. 618-625.
8. Riddle, Todd W. A Numerical Analysis of Three-Dimensional Vortex Trapping. Master's Thesis. California Polytechnic State University, San Luis Obispo, June 1992, pp. 1-29.
9. Chan, W. M. and Steger, J. L. A Generalized Scheme for Three-Dimensional Hyperbolic Grid Generation. *AIAA Paper 91-1586*, June 1991.
10. Baldwin, Barrett S. and Barth, Timothy J. A One-Equation Turbulence Transport Model. NASA TM 102847. August 1990.
11. Amtec Engineering. Tecplot User's Manual. Version 6, 1994.

APPENDIX A - EXPERIMENTAL DATA


Table 5: Physical Constants

sink strength =	$5.7 \cdot 10^{-3} \text{ m}^3/\text{s}$
chord =	0.102 m
span =	0.0635 m
kinematic viscosity =	$1.2 \cdot 10^{-5} \text{ m}^2/\text{s}$
plate thickness =	1.56 %

Column Headings for Table 6:

1. The angle of attack in degrees.
2. The horizontal distance of the sink in mm.
3. The horizontal distance of the sink in chord lengths.
4. The vertical distance of the sink in mm.
5. The vertical distance of the sink in chord lengths.
6. The minimum freestream velocity in m/s (for a stable vortex).
7. The maximum freestream velocity in m/s (for a stable vortex).
8. The minimum dimensionless sink strength (for a stable vortex).
9. The maximum dimensionless sink strength (for a stable vortex).
10. The minimum Re (for a stable vortex).
11. The maximum Re (for a stable vortex).
12. Expected values for V_{sink} to be used in INS2D.

Table 6: Raw and Reduced Data

α (°)	X	Y	V_{min} (m/s)	V_{max} (m/s)	M_{min}	M_{max}	Re_{min}	Re_{max}	$V_{\text{sink}_{\text{min}}}$	$V_{\text{sink}_{\text{max}}}$
2.50	0.10	0.10	Re-attached flow							
2.50	0.16	0.06	Re-attached flow							
2.50	0.19	0.16	Re-attached flow							
2.50	0.22	0.16	Re-attached flow							
5.00	0.06	0.06	1.00	1.50	0.585	0.878	8430	12645	0.372	0.557
5.00	0.06	0.10	Separated Flow							

5.00	0.06	0.13	1.00	1.25	0.702	0.878	8430	10537	0.446	0.557
5.00	0.10	0.10	1.25	2.00	0.439	0.702	10537	16860	0.279	0.446
5.00	0.13	0.10	2.00	2.00	0.439	0.439	16860	16860	0.279	0.279
5.00	0.16	0.10	Re-attached flow							
5.00	0.19	0.13	Re-attached flow							
5.00	0.25	0.19	1.00	1.50	0.585	0.878	8430	12645	0.372	0.557
7.50	0.00	0.05	1.00	1.50	0.585	0.878	8430	12645	0.372	0.557
7.50	0.06	0.10	1.00	2.00	0.439	0.878	8430	16860	0.279	0.557
7.50	0.10	0.10	1.25	2.00	0.439	0.702	10537	16860	0.279	0.446
7.50	0.10	0.12	1.50	2.00	0.439	0.585	12645	16860	0.279	0.372
7.50	0.22	0.10	1.25	1.50	0.585	0.702	10537	12645	0.372	0.446
7.50	0.22	0.10	Re-attached flow							
10.00	0.00	0.10	1.00	1.50	0.585	0.878	8430	12645	0.372	0.557
10.00	0.00	0.13	1.00	1.50	0.585	0.878	8430	12645	0.372	0.557
10.00	0.03	0.10	1.00	1.50	0.585	0.878	8430	12645	0.372	0.557
10.00	0.10	0.10	1.25	1.75	0.502	0.702	10537	14752	0.319	0.446
10.00	0.13	0.13	1.50	2.00	0.439	0.585	12645	16860	0.279	0.372
10.00	0.19	0.13	2.00	3.75	0.234	0.439	16860	31612	0.149	0.279
10.00	0.24	0.20	1.00	2.50	0.351	0.878	8430	21074	0.223	0.557
10.00	0.28	0.20	1.00	3.00	0.293	0.878	8430	25289	0.186	0.557
10.00	0.29	0.19	1.00	3.50	0.251	0.878	8430	29504	0.159	0.557
10.00	0.30	0.18	1.50	4.00	0.219	0.585	12645	33719	0.139	0.372
10.00	0.31	0.19	1.00	3.50	0.251	0.878	8430	29504	0.159	0.557
10.00	0.31	0.21	1.00	2.50	0.351	0.878	8430	21074	0.223	0.557
10.00	0.31	0.23	1.00	2.00	0.439	0.878	8430	16860	0.279	0.557
10.00	0.33	0.12	5.25	5.25	0.167	0.167	44256	44256	0.106	0.106
10.00	0.33	0.14	3.75	4.50	0.195	0.234	31612	37934	0.124	0.149
10.00	0.33	0.15	2.00	3.75	0.234	0.439	16860	31612	0.149	0.279
10.00	0.33	0.17	1.50	3.75	0.234	0.585	12645	31612	0.149	0.372
10.00	0.33	0.21	1.00	2.50	0.351	0.878	8430	21074	0.223	0.557
10.00	0.33	0.24	1.00	2.00	0.439	0.878	8430	16860	0.279	0.557
10.00	0.33	0.30	1.00	1.25	0.702	0.878	8430	10537	0.446	0.557
10.00	0.36	0.12	5.50	5.50	0.160	0.160	46364	46364	0.101	0.101
10.00	0.36	0.14	4.00	5.00	0.176	0.219	33719	42149	0.111	0.139

10.00	0.36	0.16	2.00	4.25	0.207	0.439	16860	35826	0.131	0.279
10.00	0.36	0.19	1.00	3.50	0.251	0.878	8430	29504	0.159	0.557
10.00	0.36	0.23	1.00	2.50	0.351	0.878	8430	21074	0.223	0.557
11.50	-0.06	0.08	Separated Flow							
15.00	0.13	0.13	1.50	2.50	0.351	0.585	12845	21074	0.223	0.372
15.00	0.24	0.20	1.00	3.00	0.293	0.878	8430	25289	0.186	0.557
15.00	0.25	0.19	1.00	2.75	0.319	0.878	8430	23182	0.203	0.557
15.00	0.28	0.15	1.25	2.25	0.390	0.702	10537	18967	0.248	0.446
15.00	0.29	0.20	1.00	3.50	0.251	0.878	8430	29504	0.159	0.557
15.00	0.31	0.20	1.00	3.50	0.251	0.878	8430	29504	0.159	0.557
15.00	0.31	0.15	2.50	2.50	0.351	0.351	21074	21074	0.223	0.223
15.00	0.31	0.18	1.00	4.00	0.219	0.878	8430	33719	0.139	0.557
15.00	0.31	0.24	1.00	2.50	0.351	0.878	8430	21074	0.223	0.557
15.00	0.33	0.21	1.00	3.75	0.234	0.878	8430	31612	0.149	0.557
15.00	0.34	0.18	4.00	5.00	0.176	0.219	33719	42149	0.111	0.139
15.00	0.35	0.20	1.00	4.25	0.207	0.878	8430	35826	0.131	0.557
15.00	0.39	0.19	1.00	3.50	0.251	0.878	8430	29504	0.159	0.557
15.00	0.39	0.23	1.00	3.00	0.293	0.878	8430	25289	0.186	0.557
15.00	0.40	0.16	2.00	4.50	0.195	0.439	16860	37934	0.124	0.279
15.00	0.42	0.18	1.25	4.50	0.195	0.702	10537	37934	0.124	0.446
15.00	0.44	0.24	1.00	3.50	0.251	0.878	8430	29504	0.159	0.557
15.00	0.45	0.16	3.00	6.50	0.135	0.293	25289	54793	0.086	0.186
15.00	0.45	0.18	3.00	5.50	0.160	0.293	25289	46364	0.101	0.186
15.00	0.45	0.19	1.25	4.75	0.185	0.702	10537	40041	0.117	0.446
15.00	0.45	0.21	1.00	4.25	0.207	0.878	8430	35826	0.131	0.557
15.00	0.46	0.12	5.00	5.00	0.176	0.176	42149	42149	0.111	0.111
15.00	0.47	0.18	1.25	5.00	0.176	0.702	10537	42149	0.111	0.446
15.00	0.47	0.21	1.00	3.00	0.293	0.878	8430	25289	0.186	0.557
20.00	0.16	0.13	1.50	3.50	0.251	0.585	12845	29504	0.159	0.372
20.00	0.24	0.18	1.00	4.00	0.219	0.878	8430	33719	0.139	0.557
20.00	0.25	0.16	1.75	4.50	0.195	0.502	14752	37934	0.124	0.319
20.00	0.27	0.17	1.50	4.25	0.207	0.585	12845	35826	0.131	0.372
20.00	0.27	0.19	1.00	4.00	0.219	0.878	8430	33719	0.139	0.557
20.00	0.27	0.21	1.00	4.00	0.219	0.878	8430	33719	0.139	0.557

20.00	0.30	0.13	3.00	3.00	0.293	0.293	25289	25289	0.186	0.186		
20.00	0.30	0.16	2.50	4.50	0.195	0.351	21074	37934	0.124	0.223		
20.00	0.30	0.19	1.00	4.00	0.219	0.878	8430	33719	0.139	0.557		
20.00	0.32	0.16	3.50	4.00	0.219	0.251	29504	33719	0.139	0.159		
25.00	0.10	0.13	1.00	1.50	0.585	0.878	8430	12645	0.372	0.557		
25.00	0.13	0.13	1.00	3.25	0.270	0.878	8430	27397	0.172	0.557		
25.00	0.23	0.18	1.00	4.00	0.219	0.878	8430	33719	0.139	0.557		
25.00	0.26	0.18	1.00	4.75	0.185	0.878	8430	40041	0.117	0.557		
25.00	0.27	0.16	1.00	4.75	0.185	0.878	8430	40041	0.117	0.557		
25.00	0.27	0.20	1.00	4.00	0.219	0.878	8430	33719	0.139	0.557		
25.00	0.28	0.14	2.50	4.50	0.195	0.351	21074	37934	0.124	0.223		
25.00	0.29	0.16	1.50	4.50	0.195	0.585	12645	37934	0.124	0.372		
25.00	0.29	0.18	1.25	4.50	0.195	0.702	10537	37934	0.124	0.446		
25.00	0.29	0.20	1.00	4.00	0.219	0.878	8430	33719	0.139	0.557		
25.00	0.31	0.18	1.00	4.50	0.195	0.878	8430	37934	0.124	0.557		
25.00	0.31	0.20	1.00	4.00	0.219	0.878	8430	33719	0.139	0.557		
25.00	0.31	0.14	1.00	4.25	0.207	0.878	8430	35826	0.131	0.557		
25.00	0.32	0.21	1.00	4.00	0.219	0.878	8430	33719	0.139	0.557		
25.00	0.33	0.19	1.00	4.25	0.207	0.878	8430	35826	0.131	0.557		
25.00	0.34	0.13	2.00	4.00	0.219	0.439	16860	33719	0.139	0.279		
25.00	0.34	0.16	1.50	4.25	0.207	0.585	12645	35826	0.131	0.372		
27.50	0.03	0.11	1.00	1.25	0.702	0.878	8430	10537	0.446	0.557		
31.50	-0.23	0.02	Separated Flow									
40.00	-0.30	0.18	1.00	1.25	0.702	0.878	8430	10537	0.446	0.557		
60.00	-0.22	-0.21	Separated Flow									

APPENDIX B - FLOW INPUT FILE

The input file AF.IN was used to pass several important parameters on to INS2D. These parameters are listed below.

Table 7: INS2D's Flow Input File (AF.IN)

Description of Variables																													
<pre> \$datain ntmax=200, niter=10, beta=20., dtau=1.0, dt=1.0, epscon=0.01, reynum=16800, iss=1, istart=0, iturb=2, ivis=4, \$end \$zonein kpr=f, \$end \$geomin alpha=20.0, vsink=.796, \$end </pre>	<table border="1"> <tbody> <tr> <td><i>ntmax</i></td> <td>Maximum number of iterations</td> </tr> <tr> <td><i>niter</i></td> <td>Display every 10th iteration</td> </tr> <tr> <td><i>beta</i></td> <td>The artificial compressibility parameter</td> </tr> <tr> <td><i>dtau</i></td> <td>Pseudo time step</td> </tr> <tr> <td><i>dt</i></td> <td>Time step</td> </tr> <tr> <td><i>epscon</i></td> <td>Minimum required divergence of velocity for a converged solution (Calculations are stopped when the maximum divergence of velocity, <i>resmax</i>, is less than <i>epscon</i>)</td> </tr> <tr> <td><i>reynum</i></td> <td>Reynolds number</td> </tr> <tr> <td><i>iss</i></td> <td>Time accurate or steady state calculation switch (<i>iss</i> = 1 for steady state)</td> </tr> <tr> <td><i>istart</i></td> <td>Starting conditions switch (<i>istart</i> = 0 for initial conditions)</td> </tr> <tr> <td><i>iturb</i></td> <td>Turbulence Model (<i>iturb</i> = 2 for Baldwin-Barth)</td> </tr> <tr> <td><i>ivis</i></td> <td>Viscous flux type switch (<i>ivis</i> = 4 for variable viscosity and non-orthogonal grid)</td> </tr> <tr> <td><i>kpr</i></td> <td>If the grid is periodic in the k-direction <i>kpr</i> = t, otherwise <i>kpr</i> = f</td> </tr> <tr> <td><i>alpha</i></td> <td>Angle of attack in degrees</td> </tr> <tr> <td><i>vsink</i></td> <td>Dimensionless sink strength</td> </tr> </tbody> </table>	<i>ntmax</i>	Maximum number of iterations	<i>niter</i>	Display every 10 th iteration	<i>beta</i>	The artificial compressibility parameter	<i>dtau</i>	Pseudo time step	<i>dt</i>	Time step	<i>epscon</i>	Minimum required divergence of velocity for a converged solution (Calculations are stopped when the maximum divergence of velocity, <i>resmax</i> , is less than <i>epscon</i>)	<i>reynum</i>	Reynolds number	<i>iss</i>	Time accurate or steady state calculation switch (<i>iss</i> = 1 for steady state)	<i>istart</i>	Starting conditions switch (<i>istart</i> = 0 for initial conditions)	<i>iturb</i>	Turbulence Model (<i>iturb</i> = 2 for Baldwin-Barth)	<i>ivis</i>	Viscous flux type switch (<i>ivis</i> = 4 for variable viscosity and non-orthogonal grid)	<i>kpr</i>	If the grid is periodic in the k-direction <i>kpr</i> = t, otherwise <i>kpr</i> = f	<i>alpha</i>	Angle of attack in degrees	<i>vsink</i>	Dimensionless sink strength
<i>ntmax</i>	Maximum number of iterations																												
<i>niter</i>	Display every 10 th iteration																												
<i>beta</i>	The artificial compressibility parameter																												
<i>dtau</i>	Pseudo time step																												
<i>dt</i>	Time step																												
<i>epscon</i>	Minimum required divergence of velocity for a converged solution (Calculations are stopped when the maximum divergence of velocity, <i>resmax</i> , is less than <i>epscon</i>)																												
<i>reynum</i>	Reynolds number																												
<i>iss</i>	Time accurate or steady state calculation switch (<i>iss</i> = 1 for steady state)																												
<i>istart</i>	Starting conditions switch (<i>istart</i> = 0 for initial conditions)																												
<i>iturb</i>	Turbulence Model (<i>iturb</i> = 2 for Baldwin-Barth)																												
<i>ivis</i>	Viscous flux type switch (<i>ivis</i> = 4 for variable viscosity and non-orthogonal grid)																												
<i>kpr</i>	If the grid is periodic in the k-direction <i>kpr</i> = t, otherwise <i>kpr</i> = f																												
<i>alpha</i>	Angle of attack in degrees																												
<i>vsink</i>	Dimensionless sink strength																												